

# Accepted Manuscript

Research papers

Factors controlling changes in evapotranspiration, runoff, and soil moisture over the conterminous U.S.: accounting for vegetation dynamics

Mingliang Liu, Jennifer C. Adam, Alexandra S. Richey, Zaichun Zhu, Ranga B. Myneni

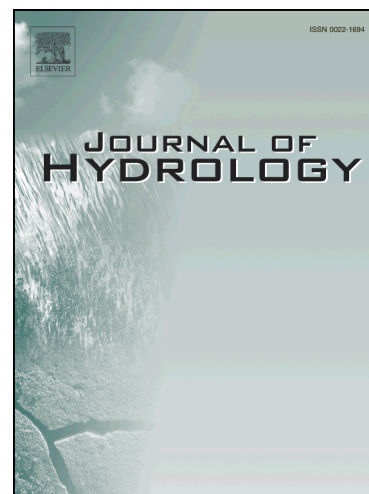
PII: S0022-1694(18)30582-1  
DOI: <https://doi.org/10.1016/j.jhydrol.2018.07.068>  
Reference: HYDROL 23000

To appear in: *Journal of Hydrology*

Received Date: 9 January 2018  
Revised Date: 23 July 2018  
Accepted Date: 26 July 2018

Please cite this article as: Liu, M., Adam, J.C., Richey, A.S., Zhu, Z., Myneni, R.B., Factors controlling changes in evapotranspiration, runoff, and soil moisture over the conterminous U.S.: accounting for vegetation dynamics, *Journal of Hydrology* (2018), doi: <https://doi.org/10.1016/j.jhydrol.2018.07.068>

This is a PDF file of an unedited manuscript that has been accepted for publication. As a service to our customers we are providing this early version of the manuscript. The manuscript will undergo copyediting, typesetting, and review of the resulting proof before it is published in its final form. Please note that during the production process errors may be discovered which could affect the content, and all legal disclaimers that apply to the journal pertain.



**Factors controlling changes in evapotranspiration, runoff, and soil moisture over the  
conterminous U.S.: accounting for vegetation dynamics**

Mingliang Liu<sup>1</sup>, Jennifer C. Adam<sup>1\*</sup>, Alexandra S. Richey<sup>1</sup>, Zaichun Zhu<sup>2</sup>, Ranga B. Myneni<sup>3</sup>

<sup>1</sup>Department of Civil and Environmental Engineering, Washington State University, Pullman,  
WA, USA;

<sup>2</sup>Sino-French Institute for Earth System Science, College of Urban and Environmental Sciences,  
Peking University, Beijing, 100871, China;

<sup>3</sup>Department of Geography and Environment, Boston University, Boston, MA, USA;

Corresponding: Adam ([jcadam@wsu.edu](mailto:jcadam@wsu.edu))

*Journal of Hydrology*

July 23, 2018

**Key points:**

1. VIC performs well in simulating streamflow, *ET*, and soil moisture over the CONUS;
2. Precipitation controls variability but not necessarily trends of water fluxes;
3. Effect of *LAI* dynamics is significant during winter season and over certain regions.

ACCEPTED MANUSCRIPT

**Abstract**

While remotely-sensed data reveal enhanced vegetation growth under a warming climate, how such vegetation dynamics could alter regional hydrology is not fully understood. In this study, we investigated how changes in leaf area index (*LAI*) and climatic variability alter long-term trends and seasonal variability of evapotranspiration (*ET*), runoff (*R*), and soil moisture (*SM*) over the conterminous United States (CONUS) during the period 1983-2009 by using the Variable Infiltration Capacity (VIC) model with transient remotely-sensed *LAI* inputs. Factor-controlled simulation experiments reveal that while precipitation is the dominant factor controlling long-term trends and inter-annual fluctuations of water fluxes, other factors (temperature, *LAI*, and atmospheric  $CO_2$ ) make significant contributions to long-term trends, particularly over specific regions. Changes in *LAI* result in minor overall contributions to the inter-annual variability of *ET*, *R*, and *SM* over the CONUS as a whole; however, they do make a more significant contribution over certain regions, such as the Midwest. Furthermore, changing *LAI* is the second most important factor in controlling variability in *ET* and *SM*, particularly over the cool season. Anomalies of *LAI* during El Nino Southern Oscillation (ENSO) phases result in no significant correlations with anomalies in *R* and *SM*, but result in positive correlations with *ET*, indicating that vegetation dynamics can have a significant impact on the hydrologic cycle over continental scales.

## 1. Introduction

The global terrestrial water cycle has been altered by environmental change and human activities especially during the last century [Hutjes *et al.*, 1998; Jackson *et al.*, 2005; Gedney *et al.*, 2006]. Concurrent to hydrologic changes, remotely-sensed data indicate an earlier greenness of vegetation and a longer growing season in the Northern Hemisphere during the last several decades due to warming, with implications for enhanced ecosystem productivity and carbon sequestration (Buermann *et al.*, 2003; Myneni *et al.*, 1997; Nemani *et al.*, 2003; Zhou *et al.*, 2001). Vegetation response to climate change (e.g., long-term warming and extreme climate events such as heat-waves and droughts) feeds back to the regional water cycle through changes in evapotranspiration (*ET*), runoff (*R*), and soil moisture (*SM*). The nature of this feedback is unclear, but is expected to vary by location and vegetation type. Feedback is known to be related to meteorology and other atmospheric variables, such as the effects of increasing atmospheric  $CO_2$  concentration on stomatal conductance and water use efficiency (Dai *et al.*, 2009; Field *et al.*, 1995; Gedney *et al.*, 2006a; Jung *et al.*, 2010; Liu *et al.*, 2013b; Wang and Dickinson, 2012).

Previous studies have highlighted the strong correlation between terrestrial *ET* and vegetation dynamics (revealed by Normalized Difference Vegetation Index - NDVI), and therefore there is a clear need to explicitly include leaf area index (*LAI*) or NDVI in *ET* estimations [e.g. Mu *et al.*, 2007; Suzuki *et al.*, 2007; Wang *et al.*, 2010a, 2010b; Yan *et al.*, 2012, 2013]. Alkama *et al.* (2010) used a modeling approach to attribute the effects of climate change,  $CO_2$  and *LAI* on long-term trends of global *R* in the 20<sup>th</sup> and 21<sup>st</sup> century. They found that stomatal conductance and vegetation growth played a minor role in the 20<sup>th</sup> century, while the role of stomatal conductance significantly increased during the 21<sup>th</sup> century. However, their study did not

investigate how these factors affect the seasonality and inter-annual variability of hydrologic processes. Shi et al. (2013, 2011) and Lei et al. (2014) investigated how these factors affect  $ET$  globally and over a mountainous catchment of China, respectively, by using the Community Land Model to simulate both  $LAI$  and hydrologic response. Similar to Alkama et al. (2010), they conclude that elevated  $CO_2$  produced negligible effects on the trend of  $R$ . Biases in simulated  $LAI$  in these studies likely result in larger uncertainties than if observed  $LAI$  had been used (Lei et al., 2014). Despite this work, there are still knowledge gaps related to how climatic factors, including temperature ( $T$ ) and precipitation ( $P$ ), interact with  $LAI$  in the context of  $CO_2$  fertilization effects on C3 vegetation (i.e., increasing stomatal resistance, therefore decreasing transpiration) and how these factors affect spatial patterns of  $ET$ ,  $R$ , and  $SM$  at regional to continental scales. In addition, the seasonality and inter-annual variability of these processes have yet to be addressed.

The Variable Infiltration Capacity (VIC) model is a macro-scale hydrologic model that has been used widely in regional and global studies of hydrology and climate change, either as an offline hydrologic model or as the land surface module within regional and global climate models (Adam et al., 2009; Hamlet et al., 2007; Hamlet and Lettenmaier, 2007; Liang et al., 1996, 1994; Liu et al., 2013b). VIC is traditionally run with constant  $LAI$  as a vegetation parameter (i.e., no year-to-year variability) such that the effects of changing phenology and inter-annual  $LAI$  variability on simulated hydrologic processes are not captured. The uncertainties from neglecting these dynamics are not well-known.

The purpose of this study is to investigate how remotely sensed vegetation changes, in combination with climate change and the  $CO_2$  fertilization effect, affect long-term and seasonal variability of terrestrial water fluxes and  $SM$  over the conterminous United States (CONUS)

during the period 1983-2009. We evaluated model simulations using observed streamflow and  $ET$ , as is commonly done [e.g. *Mote et al.*, 2005; *Xia et al.*, 2012; *Bohn et al.*, 2013; *Hamlet et al.*, 2013; *Liu et al.*, 2013b]. We also performed an additional evaluation to compare modeled water balance terms to basin-wide remotely-sensed water storage changes.

## 2. Data and Methods

### 2.1 Model description

The three-layer Variable Infiltration Capacity (VIC) model (version number 4.1.2e), with improved algorithms on snow accumulation and ablation, is used in this study (Cherkauer et al., 2003; Cherkauer and Lettenmaier, 2003, 1999; Liang et al., 1996, 1994). The VIC model is a process-based land surface and large-scale hydrologic model (Liang et al., 1994). VIC uses the variable infiltration capacity curve (Zhao et al., 1980) to simulate infiltration and overland flow, and uses Franchini and Pacciani's (1991) formula to estimate base flow. During the past decades, VIC has been improved with the implementation of multiple soil layer (Liang et al., 1996), cold-season frozen soil processes (Cherkauer et al., 2003; Cherkauer and Lettenmaier, 2003), and snowpack processes (Andreadis et al., 2009). During the past several decades, VIC has been applied and evaluated at global, continental, and large river basin scales, e.g., Elsner et al. (2010), Hamlet and Lettenmaier (1999), and Liu et al. (2013a) over the Columbia River basin (CRB), Adam et al. (2009, 2007) in the Eurasian arctic and global scale, Maurer et al. (2002) over the contiguous US, and Yuan et al. (2004) over Hanjiang River basin of China.

The control equations on energy budget and rainfall-runoff processes have been thoroughly described in VIC earlier literatures mentioned above. Here we briefly described the major pathways related to  $ET$ .  $ET$  is estimated as the total of three parts: bare soil evaporation ( $E_l$ ), wet

canopy evaporation ( $E_c$ ), and plant transpiration ( $E_t$ ) (Liang et al., 1996, 1994). All above  $ET$  components use a Penman-Monteith formulation, which is:

$$\lambda E = \frac{\Delta R_{net} + \rho_a c_p \frac{e_s - e_a}{r_a}}{\Delta + \gamma \left(1 + \frac{r_c + r_{arc}}{r_a}\right)} \quad (1)$$

where  $\lambda$  is the latent heat of vaporization [J/kg];  $E$  is evaporation [mm/s];  $\Delta$  is the slope of vapor pressure curve [Pa/K];  $R_{net}$  is the net radiation at the surface [ $W/m^2$ ];  $\rho_a$  is air density [ $kg/m^3$ ];  $c_p$  is the specific heat of moist air (1013) [J/kg/K];  $e_s$  is saturation vapor pressure [Pa];  $e_a$  is actual vapor pressure [Pa];  $r_a$  is aerodynamic resistance [s/m],  $r_{arc}$  is architectural resistance and land cover (vegetation) specific parameter [s/m], and  $r_c$  is canopy resistance [s/m];  $\gamma$  is psychrometric constant [Pa/K].

The bare soil evaporation follows the Xinanjiang model (Liang et al., 1994; Wood et al., 1992; Zhao et al., 1980), which assumes that saturated area will have the potential evaporation rate ( $E_p$ ) (setting  $r_c = 0$  in Equ. 1); and the evaporation over unsaturated area is estimated with the potential  $ET$ , fraction of saturated area, and infiltration parameter  $b$  (details can be found in Liang et al. (1994)). Evaporation from wet canopy depends on the maximum canopy evaporation ( $E_c^*$ ) and the intercepted canopy water:

$$E_c^* = \left(\frac{W_i}{W_{im}}\right)^{\frac{2}{3}} E_p \quad (2)$$

$$E_c = \min(W_i, E_c^*) \quad (3)$$

where  $W_i$  is intercepted canopy water [mm] and  $W_{im}$  is the interception capacity of canopy [mm] which is taken as a linear function of  $LAI$ . If the simulation time step is daily (i.e. 24 hours), the “ $W_i$ ” term in Equ. 3 will include the daily precipitation. The canopy transpiration (i.e.  $E_t$ ) (Equ. 4) depends on the intercepted canopy water  $W_i$ , root distribution, soil moisture, and the response

of stomatal conductance to soil moisture, temperature, and atmosphere vapor pressure deficit ( $vpd$ ) (Blondin, 1991; Ducoudre et al., 1993; Liang et al., 1994).

$$E_t = \left[ 1 - f \cdot \left( \frac{W_i}{W_{im}} \right)^{2/3} \right] \cdot E \quad (4)$$

where  $E$  is estimated from Equ. 1;  $f$  is the fraction of time for evaporating intercepted canopy water (Equ. 5), i.e.

$$f = \min \left( 1, \frac{W_i + P \cdot \Delta t}{E_c^* \cdot \Delta t} \right) \quad (5)$$

The canopy resistance for calculating  $E$  (Equ. 4) is given by (Liang et al., 1994):

$$r_c = \frac{r_{0c} \cdot g_{sm}}{LAI \cdot f(T) \cdot f(vpd)} \quad (6)$$

$$f(T) = \max(0.08 \cdot T - 0.0016T^2, 1e^{-10}) \quad (7)$$

$$f(vpd) = \max \left( 1 - \frac{vpd}{vpd_{close}}, 0.1 \right) \quad (8)$$

$$g_{sm}^{-1} = \begin{cases} 1, & W_j \geq W_j^{cr} \\ \frac{W_j - W_j^w}{W_j^{cr} - W_j^w}, & W_j^w \leq W_j \leq W_j^{cr} \\ 0, & W_j < W_j^w \end{cases} \quad (9)$$

where  $r_{0c}$  is the minimum canopy resistance and it is vegetation type specific parameter [s/m];  $g_{sm}$  is a soil moisture stress factor;  $T$  is air temperature [ $^{\circ}\text{C}$ ];  $vpd_{close}$  is the maximum  $vpd$  when stomata will be closed (here we set it as 4000 Pa) [pa];  $W_j$  is the soil moisture content in layer  $j$ ,  $j = 1, 2$ ;  $W_j^w$  is the soil moisture content at permanent wilting point, and  $W_j^{cr}$  is the critical value above which transpiration is not affected by the soil moisture. If the soil moisture in the layer that contains more than half of root, is greater than  $W_j^{cr}$ , the  $g_{sm}$  is set as 1, i.e. no water stress for transpiration; otherwise, the plant transpiration will be calculated independently for each soil and weighted by the root distribution.

## 2.2. Input Data

To drive VIC model, we applied the forcing climate data from the North American Land Assimilation System – Phase 2 (NLDAS-2, <http://ldas.gsfc.nasa.gov/nldas/NLDAS2forcing.php>), which has a spatial resolution of  $1/8^\circ$  and covers the period of 1979-2011 (hereafter NLDAS-Met). The NLDAS-Met are mainly based on North American Regional Reanalysis (NARR) (32-km spatial resolution) and have been adjusted with additional observational data, such as the monthly Parameter-elevation Regression on Independent Slopes Model (PRISM) (Daly et al., 2008; Mitchell et al., 2004; Xia et al., 2012). The calibrated parameters by Maurer et al. [2002] are used for the continental run and have been previously evaluated over the NLDAS domain (e.g. Mitchell et al., 2004; Pan et al., 2003; Sheffield et al., 2003; Xia et al., 2012).

[Insert Figure 1]

Normally, VIC uses constant monthly *LAI* (i.e., no year-to-year variability) to consider the effects of vegetation phenology on canopy conductance. Here, we enabled VIC to read in transient monthly *LAI* for each grid cell during simulation to estimate the effects of phenology on hydrologic processes. We used the 15-day Global Leaf Area Index product (*LAI3g*) with a  $1/12^\circ$  latitude-longitude resolution, which is generated from the third generation Global Inventory Modeling and Mapping Studies (GIMMS) NDVI (NDVI3g) by using a Feed-Forward Neural Network method (Tian et al., 2000; Zhu et al., 2013). In our simulations, the transient monthly *LAI* of each vegetation type in each grid cell is derived using the VIC constant monthly *LAI* parameter and the anomaly of monthly *LAI* from the *LAI3g* product (Eq. 10).

$$LAI_{y,m} = LAI_m^c \times \frac{LAI_{y,m}^{3g} - LAI_{MIN_m}^{3g}}{LAI_{MAX_m}^{3g} - LAI_{MIN_m}^{3g}} \quad (10)$$

where  $LAI^c$  represents the constant  $LAI$  value as is traditionally implemented within VIC;  $m$  represents month;  $y$  represents year;  $3g$  represents the  $LAI3g$  product;  $LAI\_MIN$  and  $LAI\_MAX$  represent the minimum, and maximum  $LAI$  during the period 1982-2011, respectively.  $LAI$  affects VIC-simulated  $ET$  through changing the amount of intercepted water in the canopy and the canopy resistance (Liang et al., 1996, 1994). The vegetation dynamics also change the seasonal patterns of  $ET$  through the distribution of roots and canopy characteristics, such as height and architectural resistance, by altering the composition of plant species within each simulation unit (i.e., each VIC grid cell). In this study, however, we just focused on the net effects of transient  $LAI$  without considering the changes in plant species and its consequent various responses to climate variability.

Annual mean atmospheric  $CO_2$  concentration is used in VIC, which is averaged from the monthly  $CO_2$  dataset at Mauna Loa Observatory ([www.esri.noaa.gov/gmd/ccgg/trends/#mlo\\_full](http://www.esri.noaa.gov/gmd/ccgg/trends/#mlo_full); last access Nov. 1, 2013). In VIC, total  $ET$  includes canopy evaporation, transpiration from leaves through stomata, and soil evaporation (Liang et al., 1996, 1994). For this study we added the effect of increasing atmospheric  $CO_2$  on maximum stomata conductance using the results of the meta-data analysis of Ainsworth and Long (2005) (as implemented by Liu et al. (2013b)), through linearly adjusting the minimum canopy resistance of all vegetation types by the same magnitude (Equ. 11):

$$f([CO_2]) = \frac{1.013}{1.35 - 0.001 \times [CO_2]} \quad (11)$$

where  $[CO_2]$  is the atmospheric  $CO_2$  concentration in ppm.

### 2.3. Factor-controlled simulation design

To separate out the contributions of climate change factors ( $T$  and  $P$ ), atmospheric  $CO_2$  concentration, and vegetation changes ( $LAI$ ), a series of factor-controlled simulation experiments

are conducted (Table 1). They include a “Transient Run” where all factors are transient, and single factor simulations where each factor ( $T$ ,  $P$ ,  $LAI$ , or atmospheric  $CO_2$  concentration) is individually fixed while all other factors are transient (Table 1). The differences in simulation results between the “Transient Run” and single factor control experiments represent the net effects (over seasonal or annual period) of that single factor on hydrologic processes in the context of interactions with other factors (Table 2; Equ. 12-15).

The “Climate” experiment represents the traditional model simulation which is driven by transient meteorological data but without changing  $LAI$  and the  $CO_2$  concentration. The mean-climate data used for fixed single-factor simulation experiments are post-processed from the transient climate data by removing the long-term trends and monthly anomalies (Hamlet and Lettenmaier, 2005; Hamlet et al., 2007; Liu et al., 2013a). All simulations start from the year of 1979, which gives us 4 years’ spin-up runs, and all current analysis are conducted for the period of 1983-2009.

The combining effect of  $CO_2$  and  $LAI$  is estimated as the difference between “Transient Run” and “Climate” runs (Equ. 16). We estimated the combining contribution of  $T$  and  $P$  (to hydrological processes) as the anomalies of simulated results from experiment “Climate”, i.e. fixed  $CO_2$  and  $LAI$  but transient  $T$  and  $P$  (Table 1; Equ. 17). The contribution of all factors is estimated with the same way (Equ. 18). To rank the contribution of each factor to the long-term trends and interannual variations of hydrological processes, the trend magnitude of their net effects and their correlations with overall variations (i.e. results of “Transient Run”) are used, respectively.

$$C(T) = f(T, P, CO_2, LAI) - f_T(P, CO_2, LAI) \quad (12)$$

$$C(P) = f(T, P, CO_2, LAI) - f_P(T, CO_2, LAI) \quad (13)$$

$$C(CO_2) = f(T, P, CO_2, LAI) - f_{CO_2}(T, P, LAI) \quad (14)$$

$$C(LAI) = f(T, P, CO_2, LAI) - f_{LAI}(T, P, CO_2) \quad (15)$$

$$C(LAI, CO_2) = f(T, P, CO_2, LAI) - f_{LAI,CO_2}(T, P) \quad (16)$$

$$C(T, P) = f_{LAI,CO_2}(T, P) - \overline{f_{LAI,CO_2}(T, P)} \quad (17)$$

$$C(T, P, CO_2, LAI) = f(T, P, CO_2, LAI) - \overline{f(T, P, CO_2, LAI)} \quad (18)$$

where  $C(factor(s))$  represents the net contribution from  $factor(s)$ ;  $f(factor(s))$  is the simulated results ( $ET$ ,  $R$ , or  $SM$ ) with transient  $factor(s)$ ; while the subscript  $factor(s)$  under the “ $f$ ”, e.g. “ $T$ ” in the term  $f_T(P, CO_2, LAI)$  represents the simulation with fixed “ $T$ ”; the items with overline represent the average during the period 1983-2009. These contributions are calculated at seasonal and annual time steps and at grid cell bases in this study.

[Insert Table 1]

## 2.4. Model evaluation

Previous VIC simulations have been extensively evaluated by comparison to historical river discharge, regional  $ET$ , snow cover and snowpack content, and water and energy budgets over the NLDAS domain (Liu et al., 2013a; Lohmann et al., 2004; Mitchell et al., 2004; Nijssen et al., 2003; Robock et al., 2003; Xia et al., 2012). Here, we reported evaluation results on river discharge both over the two largest river systems in the NLDAS domain and over small watersheds from the GAGES-II database. Comparisons between modeled results and remote

sensing products of total water content (*TWC*) and *ET* are also used for model evaluation. Due to short overlapping periods between the remote sensing data and modeled results, our comparisons are focused only on monthly and inter-annual variability and not on the trends.

Combinations of remotely sensed products and field observations have been collected for grid-by-grid or watersheds-by-watersheds model evaluations for this study. Terrestrial water storage over the land is estimated from the Gravity Recovery and Climate Experiment (GRACE) (Landerer and Swenson, 2012; Swenson and Wahr, 2006; Tapley et al., 2004) and in this study we used the Gridded GRACE *TWS anomaly* (i.e., relative to the 2004-2009 time-mean baseline) products at the spatial resolution of  $1^\circ \times 1^\circ$  from the spherical harmonic (SH) coefficients provided by the Center for Space Research (CSR, University of Texas at Austin), the Jet Propulsion Laboratory (JPL), and German Research Center for Geoscience (GFZ) centers, and scaling factors derived from NCAR's CLM4.0 (Landerer and Swenson, 2012). This product is compared to the total changes in modeled total *SM* and estimated snowpack, which we termed total water content (*TWC anomaly*). VIC does not simulate ground water dynamics and is therefore not included in the modeled *TWC anomaly*.

For *ET* evaluation, we used up-scaled *ET* from eddy-flux measurements via the model tree ensemble (MTE) method (Jung et al., 2010). For streamflow evaluation, we selected 482 USGS gages (reference watersheds) with least-disturbances from human activities (e.g., < 5% imperviousness) according to the GAGES-II (Geospatial Attributes of Gages for Evaluating Streamflow) classification (Falcone et al., 2010) (Fig.1). Each of these selected watersheds covers at least 144 km<sup>2</sup> and their monthly *R* data during the period 1990-2009 come from the USGS Hydro-Climate Data Network 2009 (HCDN-2009) dataset (Lins, 2012). Comparisons

between simulated results against remotely sensed, up-scaled products, and/or field observations are described in section 3.2.

Two observational datasets were selected to evaluate simulations of the inter-annual variability of river discharge at The Dalles station, Oregon (USGS#14105700) (outlet for the Columbia River Basin, CRB). One was reconstructed by the Climate Impacts Group at the University of Washington (UW) that uses the Bonneville Power Administration (BPA) methods (Crook, 1993); and the other dataset was reconstructed by Dai et al. (2009) with a land surface model. For the Mississippi-Atchafalaya River Basin (MARB), we selected the Mississippi-Atchafalaya River and gauge observations from USGS ([http://toxics.usgs.gov/hypoxia/mississippi/flux\\_estimates/delivery/index.html](http://toxics.usgs.gov/hypoxia/mississippi/flux_estimates/delivery/index.html)) (data availability period: 1968–2008) and Dai et al. (2009).

We divided the CONUS domain into the following six regions according to the U.S. Environment Protection Agency (<http://www.epa.gov/climatechange/impacts-adaptation/>) to report regional differences, which were also used for the third U.S. National Climate Assessment: Northeast (NE), Midwest (MW), Great Plains (GP), Northwest (NW), Southwest (SW), and Southeast (SE) (Fig. 1) (Melillo et al., 2014). We selected the two major river systems over the CONUS for evaluating simulated large-scale river discharge, i.e. the CRB and MARB (Fig. 1). The simulated river discharge over these two basins are accumulations of total annual (water year)  $R$  from contributing grid cells. VIC simulations were conducted for the NLDAS data domain from 25°N to 53°N and from 67°W to 125°W.

### 3. Results

#### 3.1. Evaluations on simulated river discharge

Comparisons between modeled results with observational and reconstructed historical data indicate that VIC, driven by the NLDAS-2 meteorological forcings and dynamic *LAI*, successfully captures the magnitude and inter-annual variability in annual river discharge, especially in the CRB. The Nash-Sutcliffe (NS) coefficients in the CRB are greater than 0.88 in comparing with both UW and Dai reconstructed data (Fig. 2). For the MARB, VIC simulated results match well with USGS observation data (NS = 0.7), but they do not match well with the reconstructed historical data from Dai et al. (2009) (Fig. 2; NS = -0.14). We did not see significant differences between the simulations with and without dynamic-*LAI* over these two basins.

[Insert Figure 2]

Over the selected reference watersheds, VIC simulated results has strong correlations with observations (with Pearson's  $r = 0.91$ ; and  $p$ -value  $\ll 0.05$ ), and the Index of Agreement (a standardized measure of the degree of model prediction error that varies between 0 and 1, 1 means perfect match; Willmott, 1981) and Mean Absolute Error are 0.95 and 139.1 mm/yr, respectively, according to the hydroGOF analysis (Fig. 3) (Zambrano-Bigiarini, 2017). While, we need to point out that the simulated results still show slight bias from the 1:1 line ( $R_{sim} = 77.3 + 0.82 \times R_{obs}$ ) (Fig. 3). Fig. 3 also reveals that by using transient *LAI* VIC provides slightly higher accuracy than traditional VIC runs (i.e. fixed *LAI*), which indicates that the widely usage of average *LAI* in regional hydrological simulations may generate some uncertainties due to kinds of non-linear responses of *LAI* to water fluxes. For inter-annual variability, VIC achieves reasonable results in terms of correlation coefficients between simulated and observed annual  $R$

(74% of watersheds have positive Pearson's  $r$  and 11.2% of total watersheds have higher  $r$  than 0.5). VIC is normally calibrated at large basin scales to study macro-scale hydrological processes at coarse spatial resolution (as in  $1/8^{\text{th}}$  degree or  $\sim 12$  km grid cell for this study). Therefore, we expected the model to perform less well over small watershed scales (i.e.  $\sim 400$  km<sup>2</sup> and less than 50,000 km<sup>2</sup>).

[Insert Figure 3]

### 3.2. Evaluations on simulated ET and total water content

Model-data comparisons reveal that VIC performs well in reconstructing the spatial patterns of multi-year average annual  $ET$  over the entire CONUS domain (Pearson's  $r = 0.98$  between VIC-simulated and MTE-derived  $ET$ ) and VIC also does reasonably well in reproducing inter-annual variability of  $ET$  ( $r = 0.67$  between VIC simulated anomalies in annual  $ET$  and the MTE-derived value; Fig. 4-a). However, VIC substantially underestimated  $ET$  for some dry years (e.g. 1988 and 2000) (Fig. 4-a). As mentioned in our previous study (i.e., Liu et al., (2013a), the missing mechanism of deep root and groundwater interaction and the irrigation effects over croplands in VIC may be the major reasons for this underestimation, although the effects of irrigation on increasing  $LAI$  are partially considered in this simulation by using observed  $LAI$  values, but are not on the increased  $ET$  that would result from additional water availability due to irrigation.

VIC does reasonably well in reproducing monthly  $TWC$  anomalies (which is accounted as the difference between transient monthly  $TWC$  and the multi-year average of  $TWC$  during the period 2004-2009; and these values represent the seasonal variability of  $TWC$ ) in comparing with

GRACE *TWS anomaly* ( $r = 0.94$ ). As to the long-term changes in the variability *TWC* (i.e., the difference between the transient monthly *TWC anomalies* (as described above) and their multi-year average monthly values during the period 2004-2009), VIC-simulated results have strong consistencies with estimates from GRACE *TWS anomalies* (with the same calculation method) ( $r = 0.6$ ; Fig. 4-b). However, because the VIC model does not explicitly model deep groundwater dynamics (nor its interactions with surface water), evaluation of VIC using GRACE *TWS anomalies* should be treated with caution.

[Insert Figure 4]

### 3.3. Long-term trends and inter-annual variability in driving forces and water fluxes

The CONUS experienced significant increases in annual mean *LAI* of  $+0.026 \pm 0.02$ /decade ( $+5.6\% \pm 4.3\%$ ) and annual mean *T* of  $+0.26 \pm 0.23^\circ\text{C}$ /decade during the period 1983-2009 (Fig. 5-a and 5-b). The range indicates the 95% confidence interval. The total annual *P* over the water year (i.e., Oct. – Sep.) had no significant trend during the study period, while it experienced a significant decrease ( $p$ -value = 0.07) in the cool season (i.e., Oct. – Mar.). Spatial trends in climate variables and *LAI* demonstrate substantial regional differences. All regions experienced large and significant increases in *LAI* except the western regions (i.e., NW and SW) (Figs. 2-a). The NE had the largest increase in annual *P* and the western regions and the SE experienced large decreases (Fig. 5-c). However, not all trends in annual *P* over each region are statistically significant. Most regions show similar warming trends during the cool and warm seasons except the MW and the GP, which experienced more warming in the cool season than in the warm season (Apr. – Sep.) (Fig. 5-b).

[Insert Figure 5]

According to simulated results (the “Transient Run”), the environmental change including climate, *LAI* and atmospheric  $CO_2$  (its concentration increased by 44.8 ppm from 342.6 to 387.4 ppm, or by 13.1%, during the simulation period) cause significant spatial variability in long-term trends, inter-annual fluctuations, and seasonal patterns of the water cycle. Although the CONUS domain as a whole shows no significant long-term trend in *ET*, *R*, and *SM* during this study period, some sub-regions exhibit statistically significant trends (Figs. 5 and 6). For example, the SW experienced a significant decrease in *ET* (Fig. 5-d) and the NW experienced a significant decrease in *SM* (Figs. 5-f and 6-d) leading to much drier soil conditions (-1.9 mm/year or -11% in total) (Figs. 5-f and 6-f). The NE experienced the largest increase in *R* while most other regions, in particular the SE and the NW, exhibit declining trends (Figs. 5-e and 6-e). The spatial patterns of *SM* and *R* trends display decreasing trends in most regions, but increases in the NE. Over the entire CONUS domain, decreases in annual *R* and *SM* occurred mainly during the cool season (Figs. 5-e and 5-f).

[Insert Figure 6]

There is substantial inter-annual variability in climate, *LAI*, and simulated water variables. Over the entire CONUS domain, annual mean *T*, *P*, and *LAI* fluctuated within the ranges of  $12.88 \pm 0.97^\circ\text{C}$  (mean  $\pm$  95% confidence intervals),  $773.6 \pm 106.6$  mm/year (or  $\pm$  13.8%), and  $1.21 \pm 0.08$  m<sup>2</sup>/m<sup>2</sup> (or  $\pm$  6.7%), respectively (Figs. 7-a, b, and c). In response, the simulated water

fluxes and  $SM$  also exhibited substantial inter-annual variability over the CONUS domain, which resulted in  $ET$ ,  $R$ , and  $SM$  varying within the ranges  $507.6 \pm 49.8$  mm/year (or  $\pm 9.8\%$ ),  $266.1 \pm 67.2$  mm/year (or  $\pm 25.3\%$ ), and  $286.8 \pm 23.4$  mm (or  $\pm 8.2\%$ ), respectively (Figs. 7-d, e, and f).

[Insert Figure 7]

### 3.4. Contributing factors to inter-annual variability and long-term trends

#### 3.4.1 Ranking of their relative contributions over the entire CONUS domain

Factor-controlled experiments indicate that  $P$  was the dominant factor controlling the inter-annual fluctuations of  $R$ ,  $ET$ , and  $SM$  (Table 2). The Pearson Correlation Coefficients ( $r$ ) between  $P$ -caused and all factor-caused variability are 0.96, 0.98, and 0.99 on  $ET$ ,  $R$ , and  $SM$ , respectively, over the CONUS domain (Fig. 8; Table 2). To the long-term trends of these hydrological variables, however, other factors (including  $LAI$ ,  $T$ , and  $CO_2$ ) made virtually identical contributions as  $P$  does (Table 2). Over the CONUS domain, changes in annual mean  $LAI$  and  $T$  increased  $ET$ , while changes in  $P$  and  $CO_2$  reduced it. The net effects of all driving forces on  $ET$  resulted in a negative trend (Table 2). All factors except  $CO_2$ , had negative effects on  $R$  which decreased by 0.61, 0.44, and 0.11 mm/year/year due to changes in  $P$ ,  $T$ , and  $LAI$ , respectively (Table 2).  $P$  was the major factor controlling  $SM$ , which decreased  $SM$  by 0.26 mm/year/year (Table 2). Overall,  $T$  and  $P$  together (i.e., Climate experiment) can explain almost all inter-annual variability and the trends of the hydrologic variables during the study period over the CONUS domain as a whole (Table 2).

According to the simulation results, the use of transient  $LAI$  (instead of the monthly static  $LAI$  that does not vary from year to year, as with traditional VIC applications) has minor overall

contributions over the CONUS as a whole to the inter-annual variability of water cycles (Figs. 2, 4, and 7; Table 2). However, transient LAI does result in more significant effects on long-term trends over the study domain and on inter-annual variabilities of hydrologic variables over certain regions (e.g. the Midwest) (Fig. 8; Table 2).

Increasing  $CO_2$  had minor effects on the inter-annual fluctuations and long-term trends in the hydrologic variables, but it almost compensated for the effects of LAI on long-term trends of  $ET$  and  $R$  over the CONUS domain (Table 2). For example, LAI caused an increase in annual  $ET$  by 0.11 mm per year, while an increase in  $CO_2$  resulted in a decrease in annual  $ET$  by 0.10 mm per year (Table 2).

[Insert Table 2]

### 3.4.2 Spatial variability of the effects of contributing factors

Each factor's contribution to long-term trends and inter-annual variability was substantially different across the study domain and in different seasons (Figs. 6 and 9). Over the majority of the CONUS domain,  $P$  was the dominant factor controlling both trends and inter-annual variability in hydrologic processes (Figs. 6 and 9). However, other factors including  $T$  and LAI also dominated long-term trends over a large number of grid cells. Long-term trends in annual  $ET$  were dominantly driven by  $P$  (78% of grid cells), while 19% and 3% of the cells were driven by  $T$  and LAI, respectively (Fig. 8). In particular,  $T$  had larger influences on long-term trends in  $ET$  over energy-limited zones such as the mountainous areas of the NW, SE, and MW; and the combined effects of LAI and  $T$  dominated over 57% of the SE region (Figs. 6-g and 9). With

regards to long-term trends in  $R$  and  $SM$ ,  $P$ 's effects were dominant for most grid cells, while around 13% of the grid cells were controlled by  $T$  and  $LAI$  (Fig. 8).

With respect to inter-annual variability,  $LAI$  was the second most important controlling factor to  $ET$  (9.2% of all grid cells) and  $SM$  (3.3% of all grid cells) (Fig. 8). In the MW, its contribution to the inter-annual variability of  $ET$  was 30% of the total area (Figs. 6-j and 8).

[Insert Figure 8]

### 3.4.3. Seasonal variability of the effects of contributing factors

Each factor's relative contributions to hydrologic cycles varied by season.  $T$  and  $LAI$ 's influences on the long-term trend of  $ET$  mainly occurred over the cool season for all regions (Fig. 8). Specifically,  $T$  and  $LAI$  together controlled  $ET$  trends over 51% and 20% of the land surface during the cool and warm seasons, respectively (Fig. 8). Relative  $T$  and  $LAI$  increase more during the cool season than during warm season (Fig. 5), which could be contributing to these results.  $LAI$  also played the second-most dominant role in the inter-annual variability of  $ET$  during the cool season; 32% of the total land area was controlled by  $LAI$  (Fig. 8). However, contributions of  $T$  and  $LAI$  to inter-annual variability in  $SM$  occurred primarily during the warm season and over the western regions (Figs. 6 and 8). In comparison to  $ET$  and  $R$ , the relative variability of total  $SM$  is lower because of its larger buffer (or storage) zone. The larger contribution of  $T$  and  $LAI$  on  $SM$  during the warm season compared to the cool season might be due to the higher rates of  $ET$  in the warm season, which lowers  $SM$ , and thus the greater warm season influence is driven by  $ET$  and manifested via  $T$  and  $LAI$ . Fig. 8 indicates that the major

contributing region to this pattern is in the western U.S., which has a drier warm season soil as compared to the cool season.

## 4. Discussions

### 4.1. Responses of vegetation to natural climate variability

As expected, our simulations demonstrate that *LAI* and its dynamics (in addition to climate change) have important effects on hydrologic processes over certain regions while it may not be significant at continental scales. We need point out that *LAI* itself is also directly controlled by climate, and it can feed back to regional climate systems and the entire hydrologic cycle (Zeng and Neelin, 2000; Zhou et al., 2003, 2001). This is supported by Figs. 9, 10, and 11, showing that anomalies in *LAI* exhibit different spatial patterns during the two non-neutral phases of the El Niño Southern Oscillation (ENSO), which can be partially explained by anomalies in *P* and *T*. Fig. 10 reveals the spatial distribution of net contribution of *LAI* and *CO<sub>2</sub>* during the El Nino (i.e. 1987, 1992, 1994, and 2002) and La Nina (i.e. 1999 and 2000) years, respectively; and their correlations with the contributions of climate factors (i.e. *T* and *P*). The bubble scatter diagrams in Fig. 10 demonstrate the correlation (or cooccurrence) between the contributions of *LAI* and *CO<sub>2</sub>* and of climate (i.e. *T* and *P*) to the anomalies through counting the number of grid cells per bin (the rounded integer) in the 2-dimension space (i.e. 2D histogram) (x-axis represents the anomalies due to climate factors and y-axis is the contribution from *LAI* and *CO<sub>2</sub>*). To investigate the impact of each forcing factors on the anomalies of hydrological processes during these ENSO cycles, 2D histogram plots are drawn over the conterminous US as Fig. 11 shows. The proportion (in percentage) of each square in Fig. 11 represents that of all grid cells over the simulation domain, how much falls in each level of the magnitude of anomalies in the driving factors (i.e. *LAI*, *T*, and *P*) and how much falls in each level of the simulated magnitude of

anomalies in hydrological variables (i.e.  $ET$ ,  $R$ , and  $SM$ ). The numeric intervals of X-axis (driving forces) and Y-axis (hydrological variables) are the same with the intervals as in Fig. 9.

During El Niño years, it is cooler and wetter over the southern US with higher  $R$ ,  $ET$ , and wetter soil. Conversely, it is drier and warmer over the Pacific Northwest with lower  $R$  and drier soil (Figs. 9 and 10). During La Niña years, cooler and wetter climate dominates over the Pacific Northwest from December to February but it is drier in the summer. The southeast experiences lower precipitation and therefore produces lower  $R$  and drier soil in these years (Figs. 9 and 10). This relationship has also been reported by Buermann et al., (2003), Zhou et al. (2003), Suzuki et al. (2007), and Yan et al. (2013). Our results corroborate those of Yan et al. (2013) and Beer et al. (2010) that  $P$  is the dominant factor controlling the spatial patterns of anomalies in water fluxes (i.e.,  $ET$  and  $R$ ) and  $SM$  in both El Niño and La Niña years (Figs. 9 and 10).

On average over the CONUS domain, anomalies of  $LAI$  in these extreme years show no significant correlation with anomalies in  $R$  and  $SM$ . However, there is a slightly positive correlation with  $ET$ , indicating that vegetation dynamics can feed back to the hydrologic cycle at the continental scale (Figs. 6 and 11). This feedback occurs when there is higher  $P$  that supports higher  $LAI$ , which then enhances  $ET$  and ultimately reduces the magnitude of  $R$ . Fig. 10 indicates that when  $T$  and  $P$  (i.e., the Climate simulation) cause an  $ET$  increase (or decrease),  $LAI$  acts to further increase (or decrease)  $ET$  during these ENSO events. This response from vegetation varies significantly over different locations and  $LAI$ 's overall contribution over the CONUS domain might be cancelled out; i.e., the  $LAI$ -caused (plus the  $CO_2$ 's smaller contribution) anomalies on hydrologic variables only explain about 5% of total anomalies (5.6% on  $ET$ , 3.1% on  $R$ , and 6.4% on  $SM$ ) driven by climate factors during the ENSO cycles (Table 3). Therefore, ENSO events cannot be considered as the most important meteorological cycling phenomenon

driving the CONUS as a whole in changing the sign of the changes in the water fluxes (e.g., during both El Niño and La Niña phases, modeled  $R$  always has negative anomalies).

[Insert Figure 9]

[Insert Figure 10]

[Insert Figure 11]

[Insert Table 3]

#### 4.2. Uncertainties

In addition to  $P$  and  $T$ , changes in solar radiation and relative humidity are important controls on vegetation dynamics and  $ET$  (Nemani et al., 2003; Wang et al., 2010b). Shi et al. (2013) found that net radiation has a significant positive correlation with  $ET$  over North America. Although the MT-CLIM algorithms (Hungerford et al., 1989; Thornton et al., 2000; Thornton and Running, 1999) that are used in VIC for estimating solar radiation and relative humidity from diurnal temperature range and precipitation perform reasonably well over most of the global land surface (Bohn et al., 2013; Mueller et al., 2011; Pierce et al., 2013), more detailed sensitivity analysis is needed to investigate how VIC responds to observed radiation, rather than indirectly driven by temperature and precipitation [Liu et al., 2013b; Mueller et al., 2013b]. The selection of different climate forcing datasets can introduce biases and uncertainties in modeled results, as also reported in other studies [e.g. Mu et al., 2012; Sheffield et al., 2012; Wang and Dickinson, 2012; Trenberth et al., 2014].

We did not model vegetation dynamics (i.e., biogeochemistry or changes between biome types) in this study, but instead use remote sensing observations of historical plant  $LAI$ . This

introduction of year-to-year changes in *LAI* while ignoring changes in other vegetation structures such as root distributions and the maximum stomatal conductance may underestimate interactions between the climate system and the land surface response (Lotsch et al., 2003). Therefore, we did not fully capture the interactions between vegetation, atmospheric processes, and the hydrologic cycle (D'Odorico et al., 2007; Zeng and Neelin, 2000). A trade-off exists between capturing these effects, e.g. (Alkama et al., 2010; Liu et al., 2012; Shi et al., 2011), and increasing the overall uncertainty of vegetation response. However, this study is an advance over other hydrologic response studies using the VIC model, which assume no inter-annual variability or long-term change in *LAI*. Generally, our simulated results indicate that increasing *LAI* can increase *ET* while decreasing *R*, which is consistent with basin thinning experiments in the Southwestern U.S. (Robles et al., 2014) and conclusions from an empirical model over the CONUS domain (Sun et al., 2014).

For this study, we used empirical equations to represent the response of stomatal conductance to increasing atmospheric  $CO_2$  concentrations. This response curve and the long-term effect of  $CO_2$  is biome- and location-specific and should be calibrated and evaluated with field observations; therefore, more uncertainty analysis is needed for further assessment (Alkama et al., 2010; Field et al., 1995; Gedney et al., 2006b; Piao et al., 2007). For example, the response of stomatal conductance and effects of deep roots and water redistribution (Yan and Dickinson, 2014) to extreme drought conditions in VIC should be well parameterized with field observations.

Another limitation of this study is that this VIC version does not take into account of groundwater dynamics, i.e. the aquifer conditions (Liang et al., 1996). Some efforts have been conducted to added groundwater component to VIC or linked with other ground water models,

such as adding SIMple Ground Model (Niu et al., 2007) to VIC by Rosenberg et al. (2013); considering the groundwater table dynamic by Liang et al. (2003); and coupling with MODFLOS models by Sridhar et al. (2017). All these above-mentioned improvements increase the capabilities of VIC in considering interactions between surface hydrological processes and groundwater and the accuracies in simulating baseflow and *ET*. Due to the complicity of characterizing the groundwater aquifers, detailed model evaluations and parameterization are still needed before applying these new improvements over continental domains. Without doubt, the development of hyper-resolution models with integrated surface-subsurface hydrological processes (e.g., ParFlow, CATHY, HydroGeoSphere, etc) may enhance our knowledge and understandings on the linkages between land, water, and atmosphere (Kollet et al., 2016; Wood et al., 2011).

## 5. Conclusions

After evaluating VIC simulations using satellite data, upscaled ET observations, and reference gage streamflow records, we concluded that VIC can successfully capture the magnitude and inter-annual variability of streamflow, *ET*, and total water content over the CONUS. By using factors control simulation experiments with VIC, we analyzed the relative contributions of climate factors (*T* and *P*), atmospheric *CO*<sub>2</sub>, vegetation dynamics, and their combining effects to long-term trends and inter-annual variability of hydrologic processes; we also discussed how these factors (partially vegetation dynamics) affect hydrological cycles during extreme climate events (i.e. ENSO in this paper). Through factor simulation experiments, we found that precipitation plays the dominant role and its Pearson's correlation coefficients with variability in *ET*, *R*, and *SM* over this region are all higher than 0.95, while other factors made significant contributions to the long-term trends, particularly during the cool season and

over certain regions such as the Southeast, the Northeast, the Midwest, and the Great Plains. Changes in *LAI* result in minor overall contributions to the inter-annual variability of the water cycle over the CONUS domain as a whole; however, they result in significant effects on the long-term trends and inter-annual variabilities of hydrologic variables over certain regions, such as the Midwest. Furthermore, transient *LAI* was the second most important factor controlling the variability of *ET* and *SM*. On average over the CONUS domain, anomalies of *LAI* during ENSO phases show no significant correlation with anomalies in *R* and *SM*. However, they have slight positive correlations with *ET*, indicating that vegetation dynamics can have a significant impact on the hydrologic cycle over continental scales.

**Acknowledgements:** We would like to thank Dr. Martin Jung (Max Planck Institute for Biogeochemistry) for providing up-scaled global *ET* data; Dr. Sean Swenson for providing GRACE land data which is supported by the NASA MEaSUREs Program and being available at <http://grace.jpl.nasa.gov>; and Dr. Ge Sun, Eastern Forest Environmental Threat Assessment Center, USDA Forest Service, for providing monthly stream observations over the GAGES-II stations. The NLDAS-2 forcing data used in this study were acquired as part of the mission of NASA's Earth Science Division and archived and distributed by the Goddard Earth Sciences (GES) Data and Information Services Center (DISC). This study has been supported by the United States Department of Agriculture (grant no.: 20116700330346 for Earth System Modeling).

## References

- Adam, J.C., Haddeland, I., Su, F., Lettenmaier, D.P., 2007. Simulation of reservoir influences on annual and seasonal streamflow changes for the Lena, Yenisei, and Ob' rivers. *J. Geophys. Res.-ATMOSPHERES* 112. <https://doi.org/10.1029/2007JD008525>
- Adam, J.C., Hamlet, A.F., Lettenmaier, D.P., 2009. Implications of global climate change for snowmelt hydrology in the twenty-first century. *Hydrol. Process.* 23, 962–972. <https://doi.org/10.1002/hyp.7201>
- Ainsworth, E.A., Long, S.P., 2005. What have we learned from 15 years of free-air CO<sub>2</sub> enrichment (FACE)? A meta-analytic review of the responses of photosynthesis, canopy. *NEW Phytol.* 165, 351–371. <https://doi.org/10.1111/j.1469-8137.2004.01224.x>
- Alkama, R., Kageyama, M., Ramstein, G., 2010. Relative contributions of climate change, stomatal closure, and leaf area index changes to 20th and 21st century runoff change: A modelling approach using the Organizing Carbon and Hydrology in Dynamic Ecosystems (ORCHIDEE) land surface model. *J. Geophys. Res.-ATMOSPHERES* 115. <https://doi.org/10.1029/2009JD013408>
- Andreadis, K.M., Storck, P., Lettenmaier, D.P., 2009. Modeling snow accumulation and ablation processes in forested environments. *Water Resour. Res.* 45. <https://doi.org/10.1029/2008WR007042>
- Beer, C., Reichstein, M., Tomelleri, E., Ciais, P., Jung, M., Carvalhais, N., Roedenbeck, C., Arain, M.A., Baldocchi, D., Bonan, G.B., Bondeau, A., Cescatti, A., Lasslop, G., Lindroth, A., Lomas, M., Luysaert, S., Margolis, H., Oleson, K.W., Rouspard, O., Veenendaal, E., Viovy, N., Williams, C., Woodward, F.I., Papale, D., 2010. Terrestrial Gross Carbon Dioxide Uptake: Global Distribution and Covariation with Climate. *SCIENCE* 329, 834–838. <https://doi.org/10.1126/science.1184984>
- Blondin, C., 1991. Parameterization of land-surface processes in numerical weather prediction, in: *Land Surface Evaporation: Measurements and Parameterization*. Springer-Verlag, New York, pp. 31–54.
- Bohn, T.J., Livneh, B., Oyler, J.W., Running, S.W., Nijssen, B., Lettenmaier, D.P., 2013. Global evaluation of MTCLIM and related algorithms for forcing of ecological and hydrological models. *Agr. Forest. Meteorol.* 38–49. <https://doi.org/10.1016/j.agrformet.2013.03.003>
- Buermann, W., Anderson, B., Tucker, C., Dickinson, R., Lucht, W., Potter, C., Myneni, R., 2003. Interannual covariability in Northern Hemisphere air temperatures and greenness associated with El Niño-Southern Oscillation and the Arctic Oscillation. *J. Geophys. Res.-ATMOSPHERES* 108. <https://doi.org/10.1029/2002JD002630>
- Cherkauer, K., Bowling, L., Lettenmaier, D., 2003. Variable infiltration capacity cold land process model updates. *Glob. Planet. Change* 38, 151–159. [https://doi.org/10.1016/S0921-8181\(03\)00025-0](https://doi.org/10.1016/S0921-8181(03)00025-0)
- Cherkauer, K., Lettenmaier, D., 2003. Simulation of spatial variability in snow and frozen soil. *J. Geophys. Res.-Atmospheres* 108. <https://doi.org/10.1029/2003JD003575>
- Cherkauer, K., Lettenmaier, D., 1999. Hydrologic effects of frozen soils in the upper Mississippi River basin. *J. Geophys. Res.-Atmospheres* 104, 19599–19610. <https://doi.org/10.1029/1999JD900337>
- Crook, A.G., 1993. *Seasonal Volumes and Statistics, Columbia River Basin, 1928-1989*. Prepared for Bonneville Power Administration.
- Dai, A., Qian, T., Trenberth, K.E., Milliman, J.D., 2009. Changes in Continental Freshwater Discharge from 1948 to 2004. *J. Clim.* 22, 2773–2792. <https://doi.org/10.1175/2008JCLI2592.1>
- Daly, C., Halbleib, M., Smith, J.I., Gibson, W.P., Doggett, M.K., Taylor, G.H., Curtis, J., Pasteris, P.P., 2008. Physiographically sensitive mapping of climatological temperature and precipitation across the conterminous United States. *Int. J. Climatol.* 28, 2031–2064. <https://doi.org/10.1002/joc.1688>

- D'Odorico, P., Caylor, K., Okin, G.S., Scanlon, T.M., 2007. On soil moisture-vegetation feedbacks and their possible effects on the dynamics of dryland ecosystems. *J. Geophys. Res.-BIOGEOSCIENCES* 112. <https://doi.org/10.1029/2006JG000379>
- Ducoudre, N., Laval, K., Perrier, A., 1993. SECHIBA, a new set of parameterizations of the hydrologic exchanges at the land atmosphere interface within the lmd atmospheric general-circulation model. *J. Clim.* 6, 248–273. [https://doi.org/10.1175/1520-0442\(1993\)006<0248:SANSOP>2.0.CO;2](https://doi.org/10.1175/1520-0442(1993)006<0248:SANSOP>2.0.CO;2)
- Elsner, M.M., Cuo, L., Voisin, N., Deems, J.S., Hamlet, A.F., Vano, J.A., Mickelson, K.E.B., Lee, S.-Y., Lettenmaier, D.P., 2010. Implications of 21st century climate change for the hydrology of Washington State. *Clim. Change* 102, 225–260. <https://doi.org/10.1007/s10584-010-9855-0>
- Falcone, J.A., Carlisle, D.M., Wolock, D.M., Meador, M.R., 2010. GAGES: A stream gage database for evaluating natural and altered flow conditions in the conterminous United States. *Ecology* 91, 621–621. <https://doi.org/10.1890/09-0889.1>
- Field, C., Jackson, R., Mooney, H., 1995. Stomatal responses to increased co<sub>2</sub> - implications from the plant to the global-scale. *Plant Cell Environ.* 18, 1214–1225. <https://doi.org/10.1111/j.1365-3040.1995.tb00630.x>
- Franchini, M., Pacciani, M., 1991. Comparative-analysis of several conceptual rainfall runoff models. *J. Hydrol.* 122, 161–219. [https://doi.org/10.1016/0022-1694\(91\)90178-K](https://doi.org/10.1016/0022-1694(91)90178-K)
- Gedney, N., Cox, P., Betts, R., Boucher, O., Huntingford, C., Stott, P., 2006a. Detection of a direct carbon dioxide effect in continental river runoff records. *Nature* 439, 835–838. <https://doi.org/10.1038/nature04504>
- Gedney, N., Cox, P., Betts, R., Boucher, O., Huntingford, C., Stott, P., 2006b. Detection of a direct carbon dioxide effect in continental river runoff records. *NATURE* 439, 835–838. <https://doi.org/10.1038/nature04504>
- Hamlet, A., Lettenmaier, D., 2005. Production of temporally consistent gridded precipitation and temperature fields for the continental United States. *J. Hydrometeorol.* 6, 330–336. <https://doi.org/10.1175/JHM420.1>
- Hamlet, A., Lettenmaier, D., 1999. Effects of climate change on hydrology and water resources in the Columbia River basin. *J. Am. WATER Resour. Assoc.* 35, 1597–1623. <https://doi.org/10.1111/j.1752-1688.1999.tb04240.x>
- Hamlet, A.F., 2011. Assessing water resources adaptive capacity to climate change impacts in the Pacific Northwest Region of North America. *Hydrol. Earth Syst. Sci.* 15, 1427–1443. <https://doi.org/10.5194/hess-15-1427-2011>
- Hamlet, A.F., Elsner, M.M., Mauger, G., Lee, S.-Y., Tohver, I., Norheim, R.A., 2013. An overview of the Columbia Basin climate change scenarios project: approach, methods, and summary of key results. *Atmosphere-Ocean* 392–415. <https://doi.org/10.1080/07055900.2013.819555>
- Hamlet, A.F., Lettenmaier, D.P., 2007. Effects of 20th century warming and climate variability on flood risk in the western U.S. *Water Resour. Res.* 43. <https://doi.org/10.1029/2006WR005099>
- Hamlet, A.F., Mote, P.W., Clark, M.P., Lettenmaier, D.P., 2007. Twentieth-century trends in runoff, evapotranspiration, and soil moisture in the western United States. *J. Clim.* 20, 1468–1486. <https://doi.org/10.1175/JCLI4051.1>
- Hungerford, R., Nemani, R., Running, S.W., Coughlan, J.C., 1989. MTCLIM - A mountain microclimate simulation-model. *USDA For. Serv. Intermt. Res. Stn. Res. Pap.* 1–52.
- Hutjes, R.W.A., Kabat, P., Running, S.W., Shuttleworth, W.J., Field, C., Bass, B., Dias, M.A.F.D.S., Avissar, R., Becker, A., Claussen, M., Dolman, A.J., Feddes, R.A., Fosberg, M., Fukushima, Y., Gash, J.H.C., Guenni, L., Hoff, H., Jarvis, P.G., Kayane, I., Krenke, A.N., Liu, C., Meybeck, M., Nobre, C.A., Oyebande, L., Pitman, A., Pielke, R.A., Raupach, M., Saugier, B., Schulze, E.D., Sellers, P.J.,

- Tenhonen, T.D., Valentini, R., Victoria, R.L., Vorosmarty, C.J., 1998. Biospheric aspects of the hydrological cycle. *J. Hydrol.* 212, 1–21. [https://doi.org/10.1016/S0022-1694\(98\)00255-8](https://doi.org/10.1016/S0022-1694(98)00255-8)
- Jackson, R., Jobbagy, E., Avissar, R., Roy, S., Barrett, D., Cook, C., Farley, K., le Maitre, D., McCarl, B., Murray, B., 2005. Trading water for carbon with biological sequestration. *Science* 310, 1944–1947. <https://doi.org/10.1126/science.1119282>
- Jung, M., Reichstein, M., Ciais, P., Seneviratne, S.I., Sheffield, J., Goulden, M.L., Bonan, G., Cescatti, A., Chen, J., de Jeu, R., Dolman, A.J., Eugster, W., Gerten, D., Gianelle, D., Gobron, N., Heinke, J., Kimball, J., Law, B.E., Montagnani, L., Mu, Q., Mueller, B., Oleson, K., Papale, D., Richardson, A.D., Rouspard, O., Running, S., Tomelleri, E., Viovy, N., Weber, U., Williams, C., Wood, E., Zaehle, S., Zhang, K., 2010. Recent decline in the global land evapotranspiration trend due to limited moisture supply. *Nature* 467, 951–954. <https://doi.org/10.1038/nature09396>
- Kollet, S., Sulis, M., Maxwell, R.M., Paniconi, C., Putti, M., Bertoldi, G., Coon, E.T., Cordano, E., Endrizzi, S., Kikinzon, E., Mouche, E., Mügler, C., Park, Y.-J., Refsgaard, J.C., Stisen, S., Sudicky, E., 2016. The integrated hydrologic model intercomparison project, IH-MIP2: A second set of benchmark results to diagnose integrated hydrology and feedbacks. *Water Resour. Res.* 53, 867–890. <https://doi.org/10.1002/2016WR019191>
- Landerer, F.W., Swenson, S.C., 2012. Accuracy of scaled GRACE terrestrial water storage estimates. *WATER Resour. Res.* 48. <https://doi.org/10.1029/2011WR011453>
- Lei, H., Huang, M., Leung, L.R., Yang, D., Shi, X., Mao, J., Hayes, D.J., Schwalm, C.R., Wei, Y., Liu, S., 2014. Sensitivity of global terrestrial gross primary production to hydrologic states simulated by the Community Land Model using two runoff parameterizations. *J. Adv. Model. EARTH Syst.* 6, 658–679. <https://doi.org/10.1002/2013MS000252>
- Liang, X., Lettenmaier, D.P., Wood, E.F., Burges, S.J., 1994. A simple hydrologically based model of land-surface water and energy fluxes for general-circulation models. *J. Geophys. Res.-Atmospheres* 99, 14415–14428. <https://doi.org/10.1029/94JD00483>
- Liang, X., Wood, E., Lettenmaier, D., 1996. Surface soil moisture parameterization of the VIC-2L model: Evaluation and modification. *Glob. Planet. Change* 13, 195–206. [https://doi.org/10.1016/0921-8181\(95\)00046-1](https://doi.org/10.1016/0921-8181(95)00046-1)
- Liang, X., Xie, Z., Huang, M., 2003. A new parameterization for surface and groundwater interactions and its impact on water budgets with the variable infiltration capacity (VIC) land surface model. *J. Geophys. Res.-ATMOSPHERES* 108. <https://doi.org/10.1029/2002JD003090>
- Lins, H.F., 2012. USGS Hydro-Climatic Data Network 2009 (HCDN–2009): U.S. Geological Survey Fact Sheet 2012–3047.
- Liu, M., Adam, J.C., Hamlet, A.F., 2013a. Spatial-temporal variations of evapotranspiration and runoff/precipitation ratios responding to the changing climate in the Pacific Northwest during 1921–2006. *J Geophys Res* 118, 380–394. <https://doi.org/10.1029/2012JD018400>
- Liu, M., Tian, H., Lu, C., Xu, X., Chen, G., Ren, W., 2012. Effects of multiple environment stresses on evapotranspiration and runoff over eastern China. *J. Hydrol.* <http://dx.doi.org/10.1016/j.jhydrol.2012.01.009>
- Liu, M., Tian, H., Yang, Q., Yang, J., Song, X., Lohrenz, S.E., Cai, W.-J., 2013b. Long-term trends in evapotranspiration and runoff over the drainage basins of the Gulf of Mexico during 1901–2008. *WATER Resour. Res.* 49, 1988–2012. <https://doi.org/10.1002/wrcr.20180>
- Lohmann, D., Mitchell, K., Houser, P., Wood, E., Schaake, J., Robock, A., Cosgrove, B., Sheffield, J., Duan, Q., Luo, L., Higgins, R., Pinker, R., Tarpley, J., 2004. Streamflow and water balance intercomparisons of four land surface models in the North American Land Data Assimilation System project. *J. Geophys. Res.-ATMOSPHERES* 109. <https://doi.org/10.1029/2003JD003517>

- Lotsch, A., Tian, Y., Friedl, M., Myneni, R., 2003. Land cover mapping in support of LAI and FPAR retrievals from EOS-MODIS and MISR: classification methods and sensitivities to errors. *Int. J. REMOTE Sens.* 24, 1997–2016. <https://doi.org/10.1080/01431160210154858>
- Maurer, E.P., Wood, A.W., Adam, J.C., Lettenmaier, D.P., Nijssen, B., 2002. A long-term hydrologically based dataset of land surface fluxes and states for the conterminous United States. *J. Clim.* 15, 3237–3251. [https://doi.org/10.1175/1520-0442\(2002\)015<3237:ALTHBD>2.0.CO;2](https://doi.org/10.1175/1520-0442(2002)015<3237:ALTHBD>2.0.CO;2)
- Melillo, J., Richmond, T., Yohe, G., 2014. *Climate Change Impacts in the United States: The Third National Climate Assessment*. U.S. Global Change Research Program.
- Mitchell, K.E., Lohmann, D., Houser, P.R., Wood, E.F., Schaake, J.C., Robock, A., Cosgrove, B.A., Sheffield, J., Duan, Q., Luo, L., Higgins, R.W., Pinker, R.T., Tarpley, J.D., Lettenmaier, D.P., Marshall, C.H., Entin, J.K., Pan, M., Shi, W., Koren, V., Meng, J., Ramsay, B.H., Bailey, A.A., 2004. The multi-institution North American Land Data Assimilation System (NLDAS): Utilizing multiple GCIP products and partners in a continental distributed hydrological modeling system. *J. Geophys. Res.-Atmospheres* 109. <https://doi.org/10.1029/2003JD003823>
- Mote, P., Hamlet, A., Clark, M., Lettenmaier, D., 2005. Declining mountain snowpack in western north America. *Bull. Am. Meteorol. Soc.* 86, 39–49. <https://doi.org/10.1175/BAMS-86-1-39>
- Mu, Q., Heinsch, F.A., Zhao, M., Running, S.W., 2007. Development of a global evapotranspiration algorithm based on MODIS and global meteorology data. *Remote Sens. Environ.* 111, 519–536. <https://doi.org/10.1016/j.rse.2007.04.015>
- Mueller, B., Hirschi, M., Jimenez, C., Ciais, P., Dirmeyer, P., Dolman, A.J., Fisher, J.B., Jung, M., Ludwig, F., Maignan, F., Miralles, D., McCabe, M.F., Reichstein, M., Sheffield, J., Wang, K., Wood, E.F., Zhang, Y., Seneviratne, S.I., 2013. Benchmark products for land evapotranspiration: LandFlux-EVAL multi-dataset synthesis. *Hydrol. Earth Syst. Sci. Discuss.* 10, 769–805.
- Mueller, B., Seneviratne, S.I., Jimenez, C., Corti, T., Hirschi, M., Balsamo, G., Ciais, P., Dirmeyer, P., Fisher, J.B., Guo, Z., Jung, M., Maignan, F., McCabe, M.F., Reichle, R., Reichstein, M., Rodell, M., Sheffield, J., Teuling, A.J., Wang, K., Wood, E.F., Zhang, Y., 2011. Evaluation of global observations-based evapotranspiration datasets and IPCC AR4 simulations. *Geophys. Res. Lett.* 38. <https://doi.org/10.1029/2010GL046230>
- Myneni, R., Keeling, C., Tucker, C., Asrar, G., Nemani, R., 1997. Increased plant growth in the northern high latitudes from 1981 to 1991. *NATURE* 386, 698–702. <https://doi.org/10.1038/386698a0>
- Nemani, R., Keeling, C., Hashimoto, H., Jolly, W., Piper, S., Tucker, C., Myneni, R., Running, S., 2003. Climate-driven increases in global terrestrial net primary production from 1982 to 1999. *SCIENCE* 300, 1560–1563. <https://doi.org/10.1126/science.1082750>
- Nijssen, B., Bowling, L., Lettenmaier, D., Clark, D., El Maayar, M., Essery, R., Goers, S., Gusev, Y., Habets, F., van den Hurk, B., Jin, J., Kahan, D., Lohmann, D., Ma, X., Mahanama, S., Mocko, D., Nasonova, O., Niu, G., Samuelsson, P., Schmakin, A., Takata, K., Verseghy, D., Viterbo, P., Xia, Y., Xue, Y., Yang, Z., 2003. Simulation of high latitude hydrological processes in the Torne-Kalix basin: PILPS phase 2(e) - 2: Comparison of model results with observations. *Glob. Planet. CHANGE* 38, 31–53. [https://doi.org/10.1016/S0921-8181\(03\)00004-3](https://doi.org/10.1016/S0921-8181(03)00004-3)
- Niu, G.-Y., Yang, Z.-L., Dickinson, R.E., Gulden, L.E., Su, H., 2007. Development of a simple groundwater model for use in climate models and evaluation with Gravity Recovery and Climate Experiment data. *J. Geophys. Res.-Atmospheres* 112. <https://doi.org/10.1029/2006JD007522>
- Pan, M., Sheffield, J., Wood, E.F., Mitchell, K.E., Houser, P.R., Schaake, J.C., Robock, A., Lohmann, D., Cosgrove, B., Duan, Q.Y., Luo, L., Higgins, R.W., Pinker, R.T., Tarpley, J.D., 2003. Snow process modeling in the North American Land Data Assimilation System (NLDAS): 2. Evaluation of model simulated snow water equivalent. *J. Geophys. Res.-Atmospheres* 108, 8850. <https://doi.org/10.1029/2003JD003994>

- Piao, S., Friedlingstein, P., Ciais, P., de Noblet-Ducoudre, N., Labat, D., Zaehle, S., 2007. Changes in climate and land use have a larger direct impact than rising CO<sub>2</sub> on global river runoff trends. *Proc. Natl. Acad. Sci. U. S. A.* 104, 15242–15247. <https://doi.org/10.1073/pnas.0707213104>
- Pierce, D.W., Westerling, A.L., Oyster, J., 2013. Future humidity trends over the western United States in the CMIP5 global climate models and variable infiltration capacity hydrological modeling system. *Hydrol Earth Syst Sci* 17, 1833–1850. <https://doi.org/doi:10.5194/hess-17-1833-2013>
- Robles, M.D., Marshall, R.M., O'Donnell, F., Smith, E.B., Haney, J.A., Gori, D.F., 2014. Effects of climate variability and accelerated forest thinning on watershed-scale runoff in southwestern USA Ponderosa Pine forests. *PLoS ONE* 9, e111092. <https://doi.org/10.1371/journal.pone.0111092>
- Robock, A., Luo, L., Wood, E., Wen, F., Mitchell, K., Houser, P., Schaake, J., Lohmann, D., Cosgrove, B., Sheffield, J., Duan, Q., Higgins, R., Pinker, R., Tarpley, J., Basara, J., Crawford, K., 2003. Evaluation of the North American Land Data Assimilation System over the southern Great Plains during the warm season. *J. Geophys. Res.-ATMOSPHERES* 108. <https://doi.org/10.1029/2002JD003245>
- Rosenberg, E.A., Clark, E.A., Steinemann, A.C., Lettenmaier, D.P., 2013. On the contribution of groundwater storage to interannual streamflow anomalies in the Colorado River basin. *Hydrol. EARTH Syst. Sci.* 17, 1475–1491. <https://doi.org/10.5194/hess-17-1475-2013>
- Sheffield, J., Pan, M., Wood, E.F., Mitchell, K.E., Houser, P.R., Schaake, J.C., Robock, A., Lohmann, D., Cosgrove, B., Duan, Q.Y., Luo, L.F., Higgins, R.W., Pinker, R.T., Tarpley, J.D., Ramsay, B.H., 2003. Snow process modeling in the North American Land Data Assimilation System (NLDAS): 1. Evaluation of model-simulated snow cover extent. *J. Geophys. Res.-Atmospheres* 108, 8849. <https://doi.org/10.1029/2002JD003274>
- Shi, X., Mao, J., Thornton, P.E., Hoffman, F.M., Post, W.M., 2011. The impact of climate, CO<sub>2</sub>, nitrogen deposition and land use change on simulated contemporary global river flow. *Geophys. Res. Lett.* 38. <https://doi.org/10.1029/2011GL046773>
- Shi, X., Mao, J., Thornton, P.E., Huang, M., 2013. Spatiotemporal patterns of evapotranspiration in response to multiple environmental factors simulated by the Community Land Model. *Environ. Res. Lett.* 8. <https://doi.org/10.1088/1748-9326/8/2/024012>
- Sridhar, V., Billah, M.M., Hildreth, J.W., 2017. Coupled Surface and Groundwater Hydrological Modeling in a Changing Climate. *Groundwater*. <https://doi.org/10.1111/gwat.12610>
- Sun, G., Caldwell, P.V., McNulty, S.G., 2014. Modeling the potential role of forest thinning in maintaining water supplies under a changing climate across the Conterminous United States. *Hydrol. Process.* under review.
- Suzuki, R., Masuda, K., Dye, D.G., 2007. Interannual covariability between actual evapotranspiration and PAL and GIMMS NDVIs of northern Asia. *REMOTE Sens. Environ.* 106, 387–398. <https://doi.org/10.1016/j.rse.2006.10.016>
- Swenson, S., Wahr, J., 2006. Post-processing removal of correlated errors in GRACE data. *Geophys. Res. Lett.* 33. <https://doi.org/10.1029/2005GL025285>
- Tapley, B., Bettadpur, S., Ries, J., Thompson, P., Watkins, M., 2004. GRACE measurements of mass variability in the Earth system. *SCIENCE* 305, 503–505. <https://doi.org/10.1126/science.1099192>
- Thornton, P., Hasenauer, H., White, M., 2000. Simultaneous estimation of daily solar radiation and humidity from observed temperature and precipitation: an application over complex terrain in Austria. *Agric. For. Meteorol.* 104, 255–271. [https://doi.org/10.1016/S0168-1923\(00\)00170-2](https://doi.org/10.1016/S0168-1923(00)00170-2)
- Thornton, P., Running, S., 1999. An improved algorithm for estimating incident daily solar radiation from measurements of temperature, humidity, and precipitation. *Agric. For. Meteorol.* 93, 211–228. [https://doi.org/10.1016/S0168-1923\(98\)00126-9](https://doi.org/10.1016/S0168-1923(98)00126-9)
- Tian, Y., Zhang, Y., Knyazikhin, Y., Myneni, R., Glassy, J., Dedieu, G., Running, S., 2000. Prototyping of MODIS LAI and FPAR algorithm with LASUR and LANDSAT data. *IEEE Trans. Geosci. REMOTE Sens.* 38, 2387–2401.

- Wang, K., Dickinson, R.E., 2012. A review of global terrestrial evapotranspiration: observation, modeling, climatology, and climatic variability. *Rev. Geophys.* 50. <https://doi.org/10.1029/2011RG000373>
- Wang, K., Dickinson, R.E., Wild, M., Liang, S., 2010a. Evidence for decadal variation in global terrestrial evapotranspiration between 1982 and 2002: 1. Model development. *J. Geophys. Res.-Atmospheres* 115. <https://doi.org/10.1029/2009JD013671>
- Wang, K., Dickinson, R.E., Wild, M., Liang, S., 2010b. Evidence for decadal variation in global terrestrial evapotranspiration between 1982 and 2002: 2. Results. *J. Geophys. Res.-Atmospheres* 115. <https://doi.org/10.1029/2010JD013847>
- Willmott, C.J., 1981. On the validation of models. *Phys. Geogr.* 184–194.
- Wood, E., Lettenmaier, D., Zartarian, V., 1992. A land-surface hydrology parameterization with subgrid variability for general-circulation models. *J. Geophys. Res.-Atmospheres* 97, 2717–2728. <https://doi.org/10.1029/91JD01786>
- Wood, E.F., Roundy, J.K., Troy, T.J., van Beek, L.P.H., Bierkens, M.F.P., Blyth, E., de Roo, A., Doell, P., Ek, M., Famiglietti, J., Gochis, D., van de Giesen, N., Houser, P., Jaffe, P.R., Kollet, S., Lehner, B., Lettenmaier, D.P., Peters-Lidard, C., Sivapalan, M., Sheffield, J., Wade, A., Whitehead, P., 2011. Hyperresolution global land surface modeling: Meeting a grand challenge for monitoring Earth's terrestrial water. *Water Resour. Res.* 47. <https://doi.org/10.1029/2010WR010090>
- Xia, Y., Mitchell, K., Ek, M., Sheffield, J., Cosgrove, B., Wood, E., Luo, L., Alonge, C., Wei, H., Meng, J., Livneh, B., Lettenmaier, D., Koren, V., Duan, Q., Mo, K., Fan, Y., Mocko, D., 2012. Continental-scale water and energy flux analysis and validation for the North American Land Data Assimilation System project phase 2 (NLDAS-2): 1. Intercomparison and application of model products. *J. Geophys. Res.-Atmospheres* 117. <https://doi.org/10.1029/2011JD016048>
- Yan, B., Dickinson, R.E., 2014. Modeling hydraulic redistribution and ecosystem response to droughts over the Amazon basin using Community Land Model 4.0 (CLM4). *J. Geophys. Res.-Biogeosciences*. <https://doi.org/10.1002/2014JG002694>
- Yan, H., Wang, S.Q., Billesbach, D., Oechel, W., Zhang, J.H., Meyers, T., Martin, T.A., Matamala, R., Baldocchi, D., Bohrer, G., Dragoni, D., Scott, R., 2012. Global estimation of evapotranspiration using a leaf area index-based surface energy and water balance model. *Remote Sens. Environ.* 124, 581–595. <https://doi.org/10.1016/j.rse.2012.06.004>
- Yan, H., Yu, Q., Zhu, Z.-C., Myneni, R.B., Yan, H.-M., Wang, S.-Q., Shugart, H.H., 2013. Diagnostic analysis of interannual variation of global land evapotranspiration over 1982–2011: Assessing the impact of ENSO. *J. Geophys. Res.-Atmospheres* 118, 8969–8983. <https://doi.org/10.1002/jgrd.50693>
- Yuan, F., Xie, Z., Liu, Q., Yang, H., Su, F., Liang, X., Ren, L., 2004. An application of the VIC-3L land surface model and remote sensing data in simulating streamflow for the Hanjiang River basin. *Can. J. REMOTE Sens.* 30, 680–690. <https://doi.org/10.5589/m04-032>
- Zambrano-Bigiarini, M., 2017. hydroGOF: Goodness-of-fit functions for comparison of simulated and observed hydrological time series. <https://doi.org/10.5281/zenodo.840087>
- Zeng, N., Neelin, J., 2000. The role of vegetation-climate interaction and interannual variability in shaping the African savanna. *J. Clim.* 13, 2665–2670. [https://doi.org/10.1175/1520-0442\(2000\)013<2665:TROVCI>2.0.CO;2](https://doi.org/10.1175/1520-0442(2000)013<2665:TROVCI>2.0.CO;2)
- Zhao, R.-J., Zhang, Y.-L., Fang, L.-R., Liu, X.-R., Zhang, Q.-S., 1980. The Xinanjiang model, in: *Hydrological Forecasting Proceedings Oxford Symposium*. IASH, pp. 351–356.
- Zhou, L., Kaufmann, R., Tian, Y., Myneni, R., Tucker, C., 2003. Relation between interannual variations in satellite measures of northern forest greenness and climate between 1982 and 1999. *J. Geophys. Res.-ATMOSPHERES* 108. <https://doi.org/10.1029/2002JD002510>
- Zhou, L., Tucker, C., Kaufmann, R., Slayback, D., Shabanov, N., Myneni, R., 2001. Variations in northern vegetation activity inferred from satellite data of vegetation index during 1981 to 1999. *J. Geophys. Res.-ATMOSPHERES* 106, 20069–20083. <https://doi.org/10.1029/2000JD000115>

Zhu, Z., Bi, J., Pan, Y., Ganguly, S., Anav, A., Xu, L., Samanta, A., Piao, S., Nemani, R.R., Myneni, R.B., 2013. Global Data Sets of Vegetation Leaf Area Index (LAI)<sub>3g</sub> and Fraction of Photosynthetically Active Radiation (FPAR)<sub>3g</sub> Derived from Global Inventory Modeling and Mapping Studies (GIMMS) Normalized Difference Vegetation Index (NDVI)<sub>3g</sub> for the Period 1981 to 2011. *REMOTE Sens.* 5, 927–948. <https://doi.org/10.3390/rs5020927>

ACCEPTED MANUSCRIPT

**Table and Figure list.**

**Table 1** Simulation experiments

**Table 2** Contributions of climate factors, *LAI*, and atmospheric  $CO_2$  to the long-term and inter-annual variability of *ET*, *R*, and *SM* during the period 1983-2009 over the Conterminous US

**Table 3** Average anomalies of *ET*, *R*, and *SM* over the CONUS as driven by various factors during ENSO cycles

**Figure 1.** Study domain and the distribution of the selected watersheds from GAGES-II data sets.

The background color map is the modeled average annual *R* during the period 1983-2011. The red lines are the boundaries of GAGES-II watersheds. The dark lines are the study region boundaries. The white and pink polygons represent the Columbia River Basin (CRB) and Mississippi-Atchafalaya River Basin (MARB), respectively.

**Figure 2.** Comparisons of VIC modeled river discharges against reconstructed historical river discharge and observations for the Columbia and Mississippi-Atchafalaya Rivers. The reconstructed-Dai data are from Dai et al. (2009); the reconstructed-UW data are from the Climate Impacts Group at the University of Washington (Crook, 1993; Hamlet, 2011).

**Figure 3.** Comparisons between VIC simulated *R* and gages observations from GAGES-II database. The black and red lines are the linear regressions of simulated results from “Transient” and “FixLAI” run, respectively, with observations. The black and red triangles represent each gages sites and the corresponding simulated watersheds. The right panel is the “zooming in” of the left panel in the range of 0-1000 mm/year.

**Figure 4.** Comparisons of VIC-modeled results with remote sensing-based estimates over the conterminous US during the period 1983-2009: a) modeled anomalies in annual *ET* against up-scaled *ET* from eddy-flux stations (MTE); and b) modeled anomalies in total water content (total soil water content plus snowpack equivalent water) against GRACE-derived terrestrial water

equivalent (the square and triangle are annual mean values from GRACE and VIC, respectively). Anomalies of  $ET$  are calculated as the difference between transient annual  $ET$  and the multi-year average  $ET$  during the period 1983-2009 (panel a); Changes in TWC anomalies are calculated as the difference between the transient monthly  $TWC$  anomalies (which is counted as the difference between transient monthly  $TWC$  and the multi-year average of  $TWC$  and their multi-year average monthly values during the period 2004-2009) . Green dotted lines represent VIC simulated results with transient  $LAI$  (i.e. “Transient Run”) and Red lines represent VIC simulated results with fixed  $LAI$  (i.e. “FixLAI” experiment). In panel b, the GRACE-Ann, VIC-Ann, and Fix-LAI-VIC-Ann are the average of monthly anomalies at the annual basis.

**Figure 5.** Trends in observed annual mean  $T$ , annual  $P$ , and  $LAI$ ; and trends in simulated annual mean  $ET$ ,  $R$ , and  $SM$  over each region of the conterminous US during the period 1983-2009. The blue bar represents the cool season (October - March); the red bar represents warm season (April - September), and the black bar is the water year average. The asterisk over each bar represents a significant trend ( $t$ -test  $p$ -value  $< 0.1$ ). Error bars indicate the 95% confidence intervals of the linear trends.

**Figure 6.** On the left are trends in controlling factors (including  $T$ ,  $P$ ,  $LAI$ ) and simulated  $ET$ ,  $R$ , and  $SM$  (a-f). On the right are spatial maps of the dominant factors controlling hydrologic long-term trends (g-i) and inter-annual variability (j-l). The dominant factor controlling a long-term trend is the factor that generated the largest absolute linear trend; the dominant factor controlling inter-annual variability is the factor that produced the highest Pierce Correlation coefficient with the “Base Run” (all factors). Blue, red, green, and pink colors indicate that the long-term trend or inter-annual variability is dominantly controlled by  $P$ ,  $T$ ,  $LAI$ , and atmospheric  $CO_2$  concentration, respectively.

**Figure 7.** Anomalies (from a baseline period of 1983-2009) in annual mean  $T$ ,  $P$ ,  $LAI$ , and simulated  $ET$ ,  $R$ , and  $SM$ . Different colored bars in the right panel represent the effects of each factor on inter-annual variability: blue:  $P$ , red:  $T$ , pink:  $CO_2$ , and green:  $LAI$ . The black line shows the total effects (i.e., simulated results from “Transient Run” and displayed as anomalies).

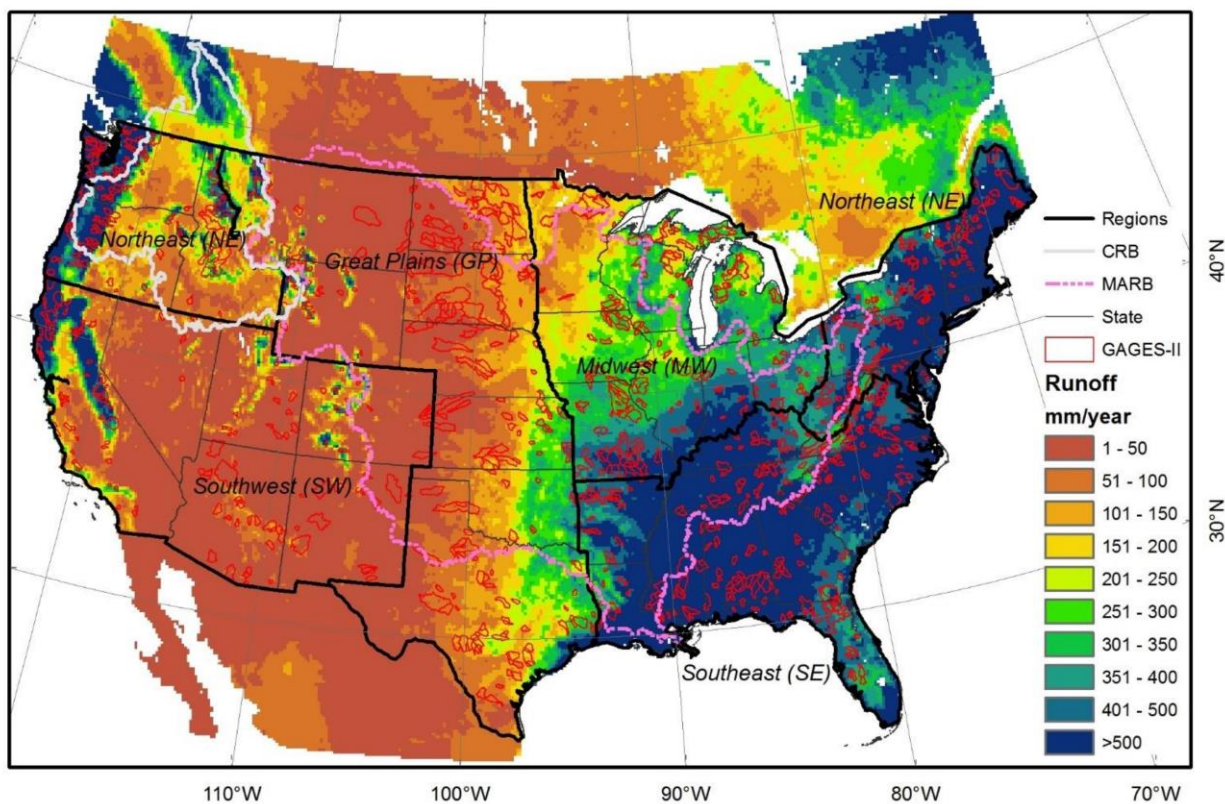
**Figure 8.** Proportion of land surface area that is dominantly controlled by each environmental factor on long-term trends and inter-annual variability of seasonal and annual  $ET$ ,  $R$ , and  $SM$  over the CONUS during the period 1983-2009.

Factors:  $LAI$ ,  $T$ ,  $P$ , and  $CO_2$ ; Hydrological processes:  $ET$ ,  $SM$ , and  $R$ ; Periods: Col (cool season: Oct. – Mar.), Wam (warm season: Apr. – Sep.), and Ann (water year: Oct. – Sep.). The value over each bar represents the percentage of grid cells that were dominantly controlled by that factor (i.e. the largest slope in long-term trend and the highest correlation coefficient with results from “Transient run”). The left panel is over entire CONUS domain and the right panel is for each region.

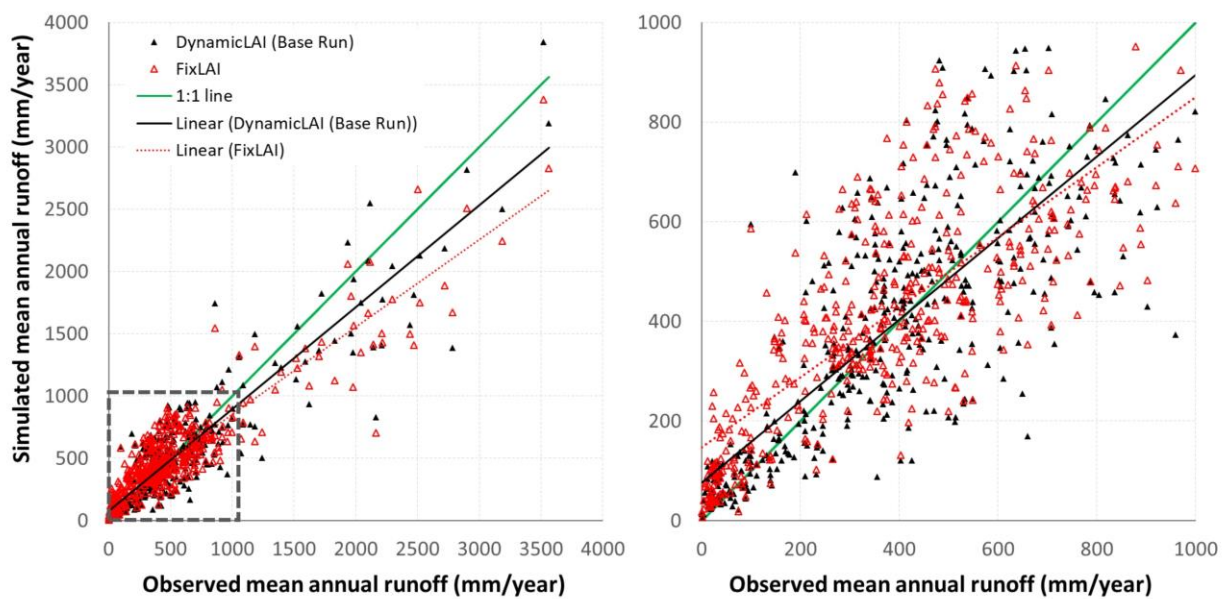
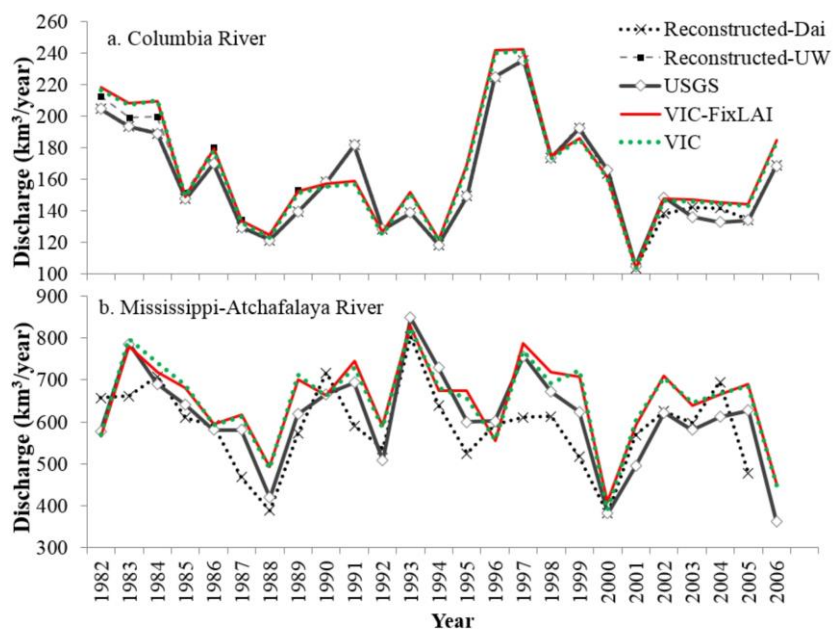
**Figure 9.** Anomalies of  $LAI$ , annual mean  $T$ , annual  $P$ , estimated  $R$ ,  $ET$ , and  $SM$  during El Niño (1987, 1992, 1994, and 2002) and La Niña events (1999 and 2000).

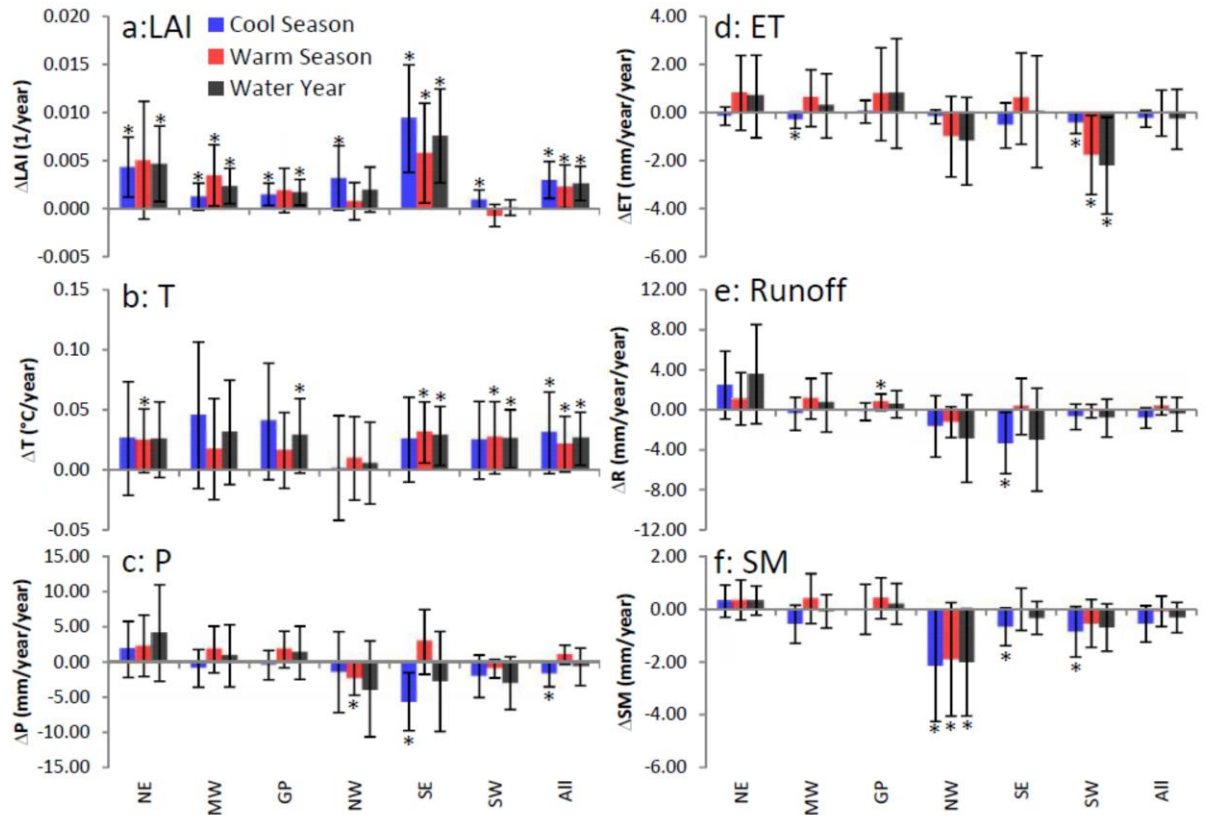
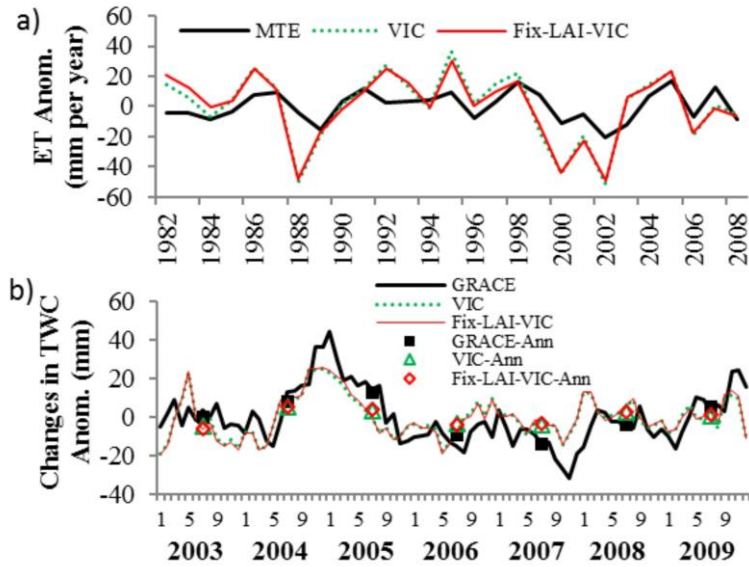
**Figure 10.** Combined contributions of transient  $LAI$  and  $CO_2$  on the  $ET$ ,  $SM$ , and  $R$  during El Niño and La Niña years (the maps) and their correlations with the contributions of climate factors (i.e.  $T$  and  $P$ ) (2D histogram plots). The red lines in the bubble diagrams represents the linear trend.

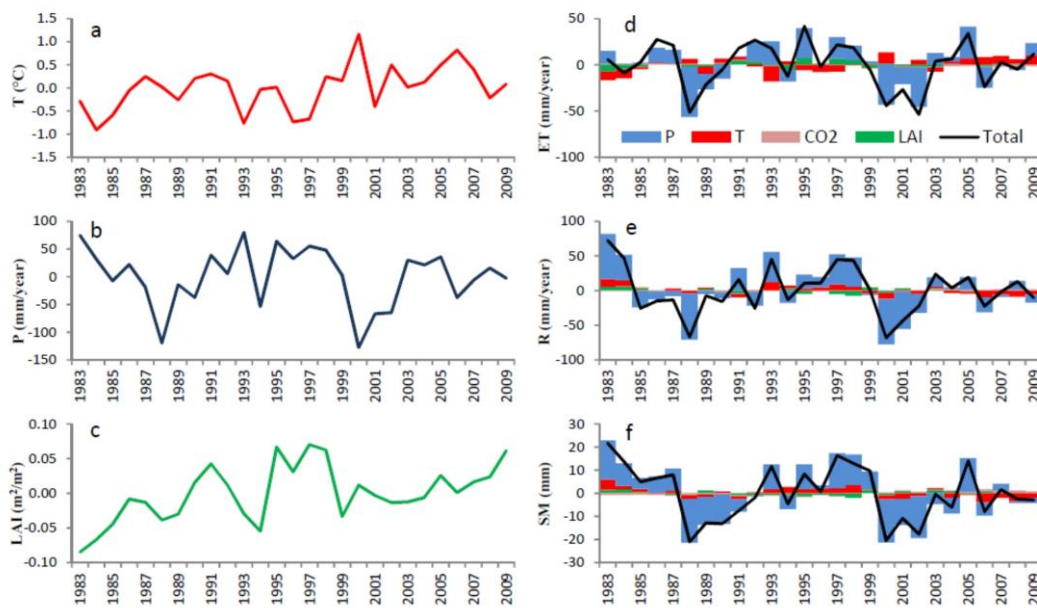
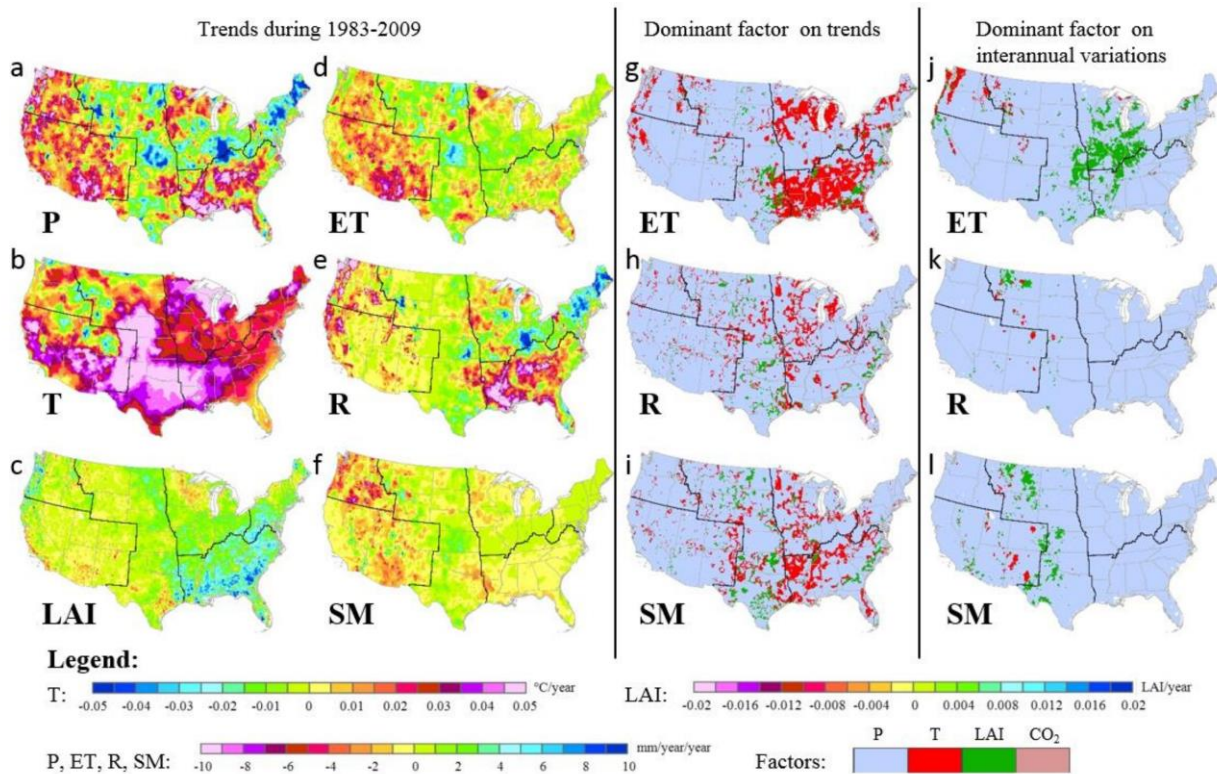
**Figure 11.** The correlations between hydrological processes and the driving factors in anomalies during the typical El Nino and La Nina years indicated by the 2D histogram plot over the conterminous US (i.e. the proportion of grid cells within each scale of anomalies in  $ET$ ,  $R$ , and  $SM$  [rows, or Y-axis] in corresponding to each scale of anomalies in driving forces [columns, or X-axis]).

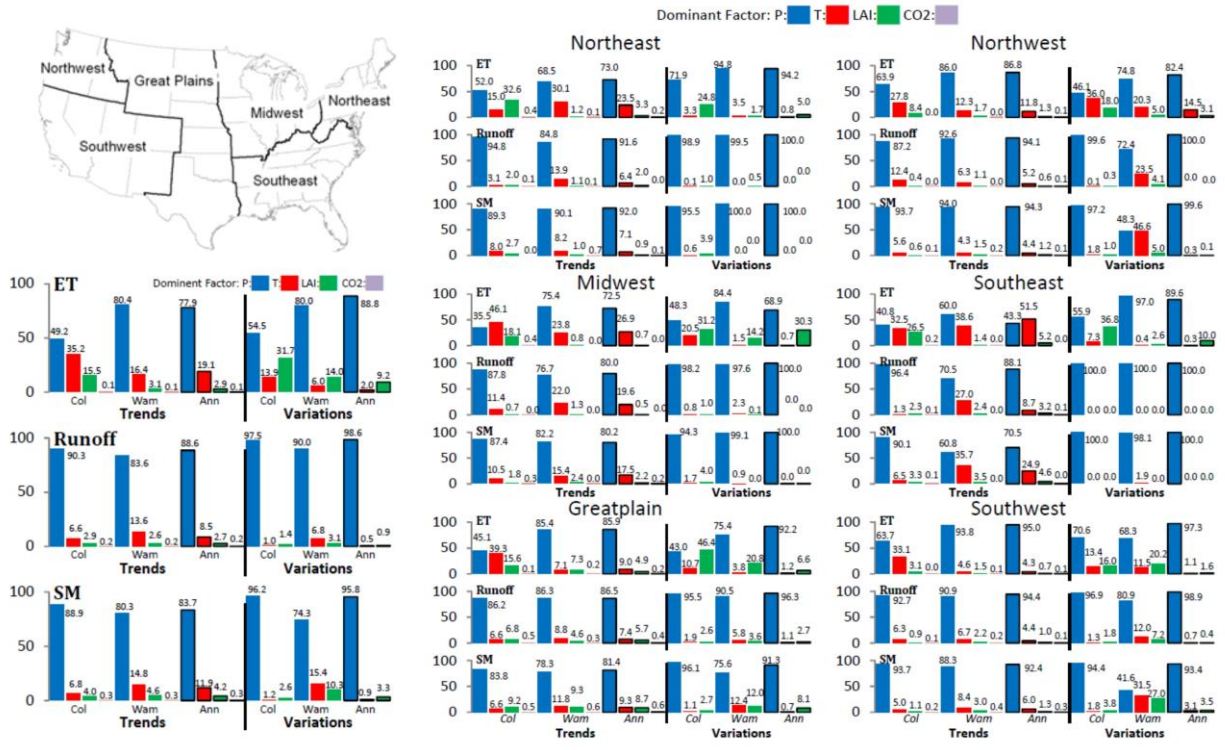


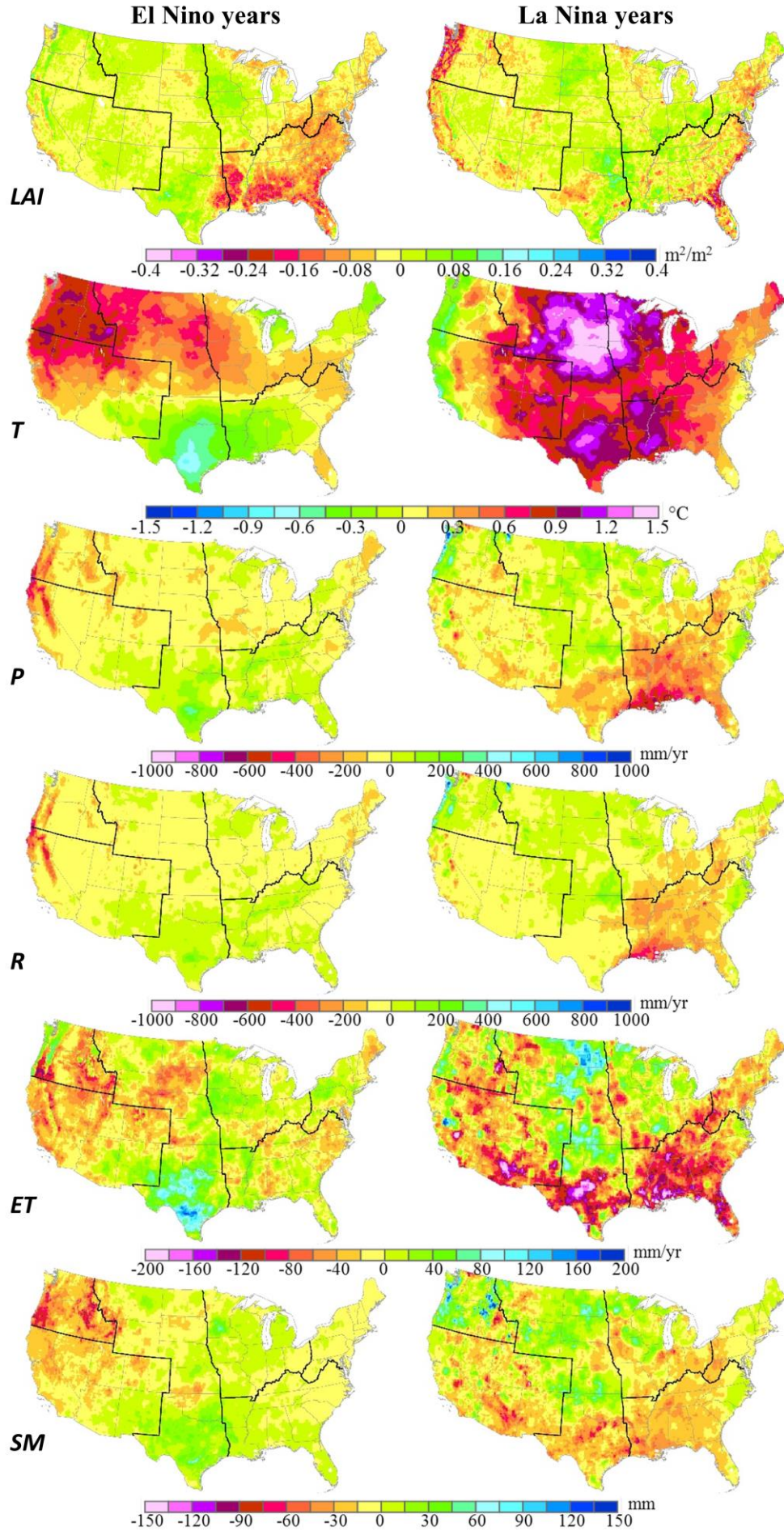
ACCEPTED

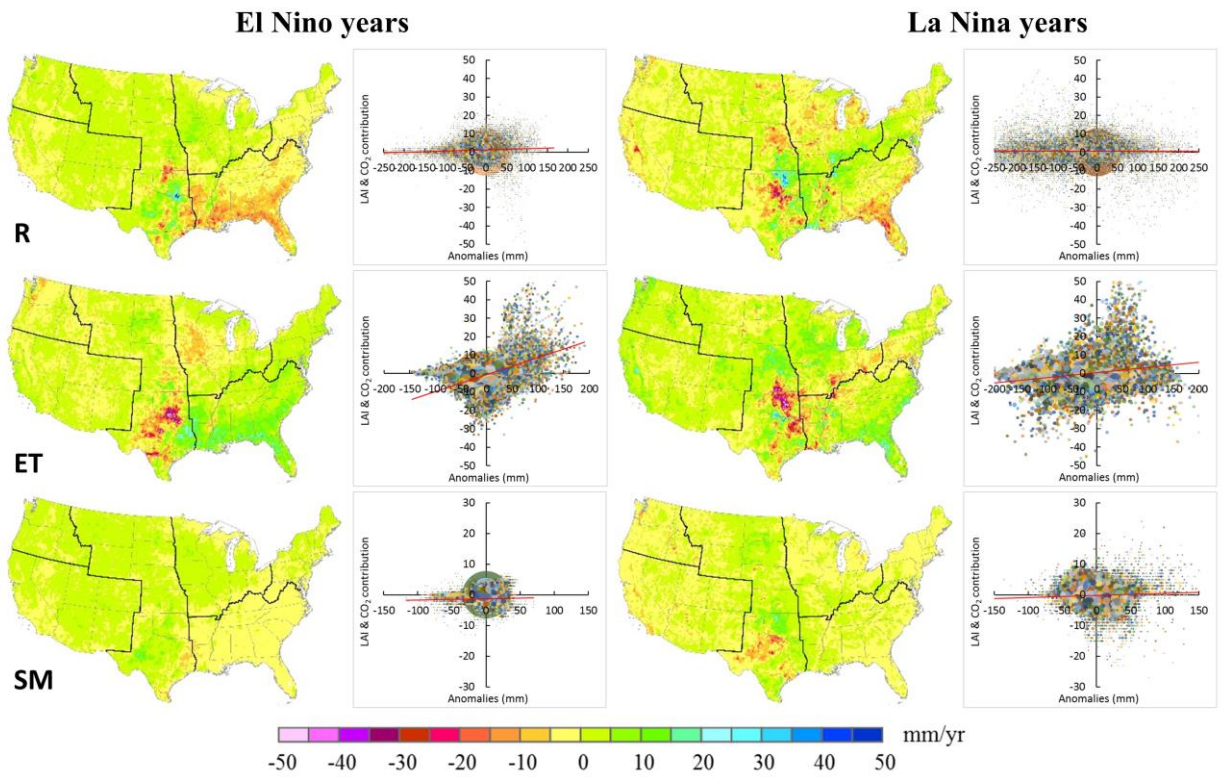




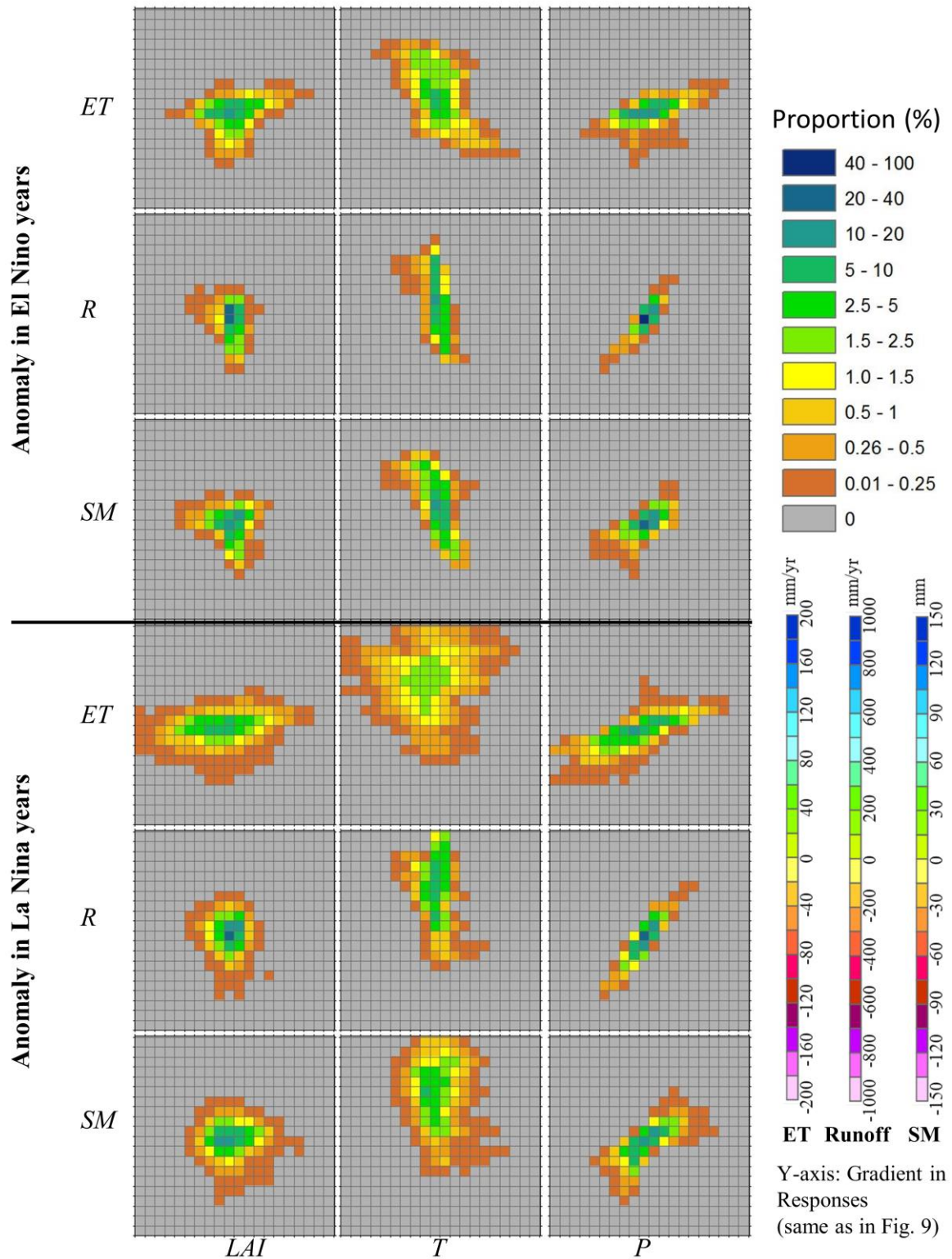








ACCEPTED



X-axis: Gradient in Driving Forces (same as in Fig. 9)

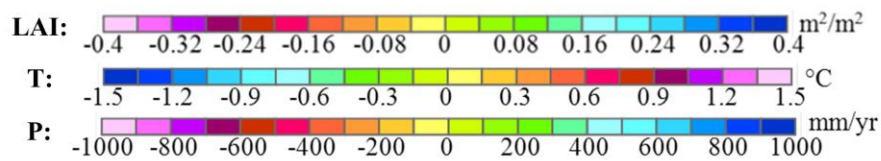


**Table 1 Simulation experiments**

Name of Experiments	Control Factors			
	<i>T</i>	<i>P</i>	<i>LAI</i>	<i>CO<sub>2</sub></i>
Transient Run	Tr	Tr	Tr	Tr
Fix <i>T</i>	M	Tr	Tr	Tr
Fix <i>P</i>	Tr	M	Tr	Tr
Fix <i>CO<sub>2</sub></i>	Tr	Tr	Tr	M
Fix <i>LAI</i>	Tr	Tr	M	Tr
Climate	Tr	Tr	M	M

Abbreviations: Tr: Transient data, i.e. annual data; M: Mean-climate during 1983-2009, or constant atmospheric *CO<sub>2</sub>* in 1983, or *LAI* in 1983.

**Table 2 Contributions of climate factors, *LAI*, and atmospheric *CO<sub>2</sub>* to the long-term and inter-annual variability of *ET*, *R*, and *SM* during 1983-2009 over the Conterminous US**

Variables	Factors						
		<i>T</i>	<i>P</i>	<i>T &amp; P</i>	<i>CO<sub>2</sub></i>	<i>LAI</i>	All
<i>ET</i>	Trend (mm/year/year)	0.46	-0.09	-0.39	-0.10	0.11	-0.28
	<i>t</i> -test for linear trend ( <i>p</i> -value)	0.00*	0.87	0.51	0.00*	0.23	0.66
	Pearson's correlation coefficient <sup>#</sup>	-0.33	0.96	0.99	-0.12	0.49	-
<i>R</i>	Trend (mm/year/year)	-0.44	-0.61	-0.32	0.10	-0.11	-0.43
	<i>t</i> -test for linear trend ( <i>p</i> -value)	0.00*	0.47	0.71	0.00*	0.20	0.62
	Pearson's correlation coefficient <sup>#</sup>	0.65	0.98	1.00	0.05	0.00	-
<i>SM</i>	Trend (mm/year/year)	-0.16	-0.26	-0.31	0.06	0.00	-0.32
	<i>t</i> -test for linear trend ( <i>p</i> -value)	0.00*	0.34	0.29	0.00*	0.98	0.28

Pearson's correlation coefficient <sup>#</sup>	0.66	0.99	1.00	-0.17	-0.08	-
--	------	------	------	-------	-------	---

Note:

#: the correlation coefficient is calculated between the single factor-caused annual anomalies and the all factor-caused (i.e. the “Transient Run”) annual anomalies. The trend driven by each factor is calculated as the differences between Base Run and each Fix factor experiment (Table 1) while contributions from *T* & *P* is directly from “Climate” simulation results.

\*: indicates a 5% level of significance (i.e.  $p$ -value < 0.05).

**Table 3** Average anomalies of *ET*, *R*, and *SM* over the CONUS as driven by various factors during ENSO cycles

Periods	Variables	Anomalies driven by factors (mm/year)	
		<i>T</i> & <i>P</i>	<i>LAI</i> & <i>CO</i> <sub>2</sub>
La Niña	<i>ET</i>	-24.0	-0.7
	<i>R</i>	-32.8	0.7
	<i>SM</i>	-4.7	0.5
El Niño	<i>ET</i>	-4.1	-0.3
	<i>R</i>	-18.0	0.7
	<i>SM</i>	-3.5	-0.1